SCIENCE CHINA
Earth Sciences

•REVIEW•

September 2020 Vol.63 No.9: 1248–1267
https://doi.org/10.1007/s11430-019-9614-y

Theory of three-pattern decomposition of global atmospheric circulation

Shujuan HU*, Bingqian ZHOU, Chenbin GAO, Zhihang XU, Qingwan WANG & Jifan CHOU

Key Laboratory for Semi-Arid Climate Change of the Ministry of Education, College of Atmospheric Sciences, Lanzhou University, Lanzhou 730000, China

Received September 29, 2019; revised March 26, 2020; accepted April 17, 2020; published online June 23, 2020

Abstract This paper reviews the three-pattern decomposition of global atmospheric circulation (3P-DGAC) developed in recent years, including the decomposition model and the dynamical equations of global horizontal, meridional, and zonal circulations. Compared with the traditional two-dimensional (2D) circulation decomposition method, the 3P-DGAC can effectively decompose the actual vertical vorticity into two components that are caused by the horizontal circulation and convergent/divergent movement (associated with the meridional and zonal circulations). It also decomposes the vertical velocity into the components of the meridional vertical circulation and the zonal vertical circulation, thus providing a new method to study the dynamical influences of convergent/divergent motions on the evolution of actual vertical vorticity and an accurate description of local vertical circulations. The 3P-DGAC is a three-dimensional (3D) circulation decomposition method based on the main characteristics of the actual atmospheric movements. The horizontal, meridional, and zonal circulations after the 3P-DGAC are the global generalization of Rossby waves in the middle-high latitudes and Hadley and Walker circulations in low latitudes. Therefore, the three-pattern decomposition model and its dynamical equations provide novel theoretical tools for studying complex interactions between middle-high and low latitude circulations as well as the physical mechanisms of the abnormal evolution of large-scale atmospheric circulations under the background of global warming.

Keywords Horizontal circulation, Meridional circulation, Zonal circulation, Three-pattern decomposition of global atmospheric circulation (3P-DGAC), Dynamical equations

Citation: Hu S, Zhou B, Gao C, Xu Z, Wang Q, Chou J. 2020. Theory of three-pattern decomposition of global atmospheric circulation. Science China Earth Sciences, 63: 1248–1267, https://doi.org/10.1007/s11430-019-9614-y

1. Introduction

Atmospheric motion on the rotating earth occurs within a gravitational field and the Coriolis force field. Its inherent properties determine that large-scale motion in the middle-high latitudes has the characteristics of quasi-hydrostatic equilibrium, quasi-geostrophic equilibrium, non-divergence, and quasi-horizontal motion (Holton and Staley, 1973). The theory of hydrostatic equilibrium, geostrophic equilibrium, and the representation of stream and potential functions in the decomposition of two-dimensional (2D) velocity field in hydrodynamics are introduced into the equations of atmospheric motion (Holton and Staley, 1973). The resulting quasi-geostrophic theory has become the theoretical basis of weather forecasts and the core theory of atmospheric dynamics (Tao et al., 2012), which enables us to understand the physical mechanisms of the generation and development of large-scale systems in middle-high latitudes deeply (Zhou et al., 2013). However, in the tropics, atmospheric motion is constrained by the conservation of angular momentum, and

* Corresponding author (email: hushuju@lzu.edu.cn)

vertical overturning motions are easily initiated. These are typically represented by Hadley and Walker circulations (Hartmann, 1994). Nevertheless, quasi-geostrophic theory is not applicable to atmospheric motion in low latitudes, which leads to the current study of atmospheric dynamics being divided into middle-high latitude atmospheric dynamics and low latitude atmospheric dynamics (Holton and Staley, 1973). However, from a global perspective, atmospheric motion around the earth should be considered as a whole. Weather systems in low latitudes are related to those in middle-high latitudes, and there are complex interactions between them. Therefore, a key scientific problem is an analysis of three-dimensional (3D) movements between middle-high and low latitude atmospheric circulations, from a global perspective (Cheng, 2019).

The most important form of large-scale motion at middle-high latitudes is the Rossby wave (Rossby, 1939). Rossby wave, with quasi-horizontal, non-divergent, and quasi-geostrophic properties, is one of the greatest discoveries in modern dynamic meteorology. They are comprised of a trough-ridge and high-low pressure system that develops after the disturbance of zonal airflow. The locations and strengths of these waves' activity centers reflect the characteristics of atmospheric circulations in the vast surrounding area. In contrast, the meridional Hadley circulation and the zonal Walker circulation dominate the overturning motions in low latitudes. Hadley circulation is considered to be the most important circulation affecting the balance of various physical variables in the global atmosphere, while the anomalous evolution of Walker circulation is regarded as a part of the phenomenon of El Niño and the Southern Oscillation (ENSO) in tropical areas. These three circulations are the most important large-scale circulations in global atmospheric flows. Their activities and changes play an essential role in global atmospheric circulation as well as in the exchange of heat and vapor between high and low latitudes, and between oceans and continents, thus exerting a major impact on the formation and evolution of weather and climate (Chelton and Schlax, 1996; England et al., 2014; Trenberth and Stepaniak, 2003; Kosaka and Xie, 2013; Guan et al., 2019).

In the context of global warming, these global large-scale circulation systems have undergone significant inter-decadal changes in the past few decades. For example, the boreal winter Hadley circulation shows a clear strengthening trend (Hu et al., 2005; Mitas and Clement, 2005), with the poleward movement of its descending branch (Hu and Fu, 2007; Hu Y Y et al., 2018), indicating a poleward expansion of the tropical and subtropical jet stream. Conversely, the Walker circulation shows a weakening trend, with the ascending branch shifting eastward (Bayr et al., 2014; DiNezio et al., 2013). Inter-decadal variations of large-scale circulations will cause global climate zones to move and change, and extreme weather and climate events will be more frequent, which may result in greater economic losses to society. The inter-decadal evolution of the intensity and location of these global large-scale atmospheric circulations and their impacts on global and local climate have become important scientific issues in the 21st century. Although a lot of effort has been devoted to this topic, we do not have a unified conclusion about the physical mechanism of the inter-decadal variations of these large-scale circulations yet.

There are complex interactions among horizontal, meridional and zonal circulations. For example, both the analysis of observations and the study of model simulations show that Rossby waves in the middle-high latitudes can propagate to the tropics at low latitudes, thus affecting the weather and climate change in the tropics (Kiladis and Weickmann, 1992a, 1992b; Kiladis and Feldstein, 1994; Kiladis and Weickmann, 1997), while the Hadley and Walker circulations in low latitudes are closely related to global atmospheric circulation anomalies. Therefore, it is very important to study the complex interactions between atmospheric circulations at low latitudes and those at middle-high latitudes (Charney, et al. 1969; Zhang and Webster, 1992; Kiladis and Weickmann, 1992a, 1992b; Kiladis and Feldstein, 1994; Kiladis and Wheeler, 1995). Although many studies have been undertaken in this field, the dynamical mechanisms of interactions among these large-scale circulations around the globe remain poorly understood.

To explore the dynamical method related to the unified description of global atmospheric circulation, Chou and his co-authors (Xu, 2001; Hu, 2006, 2008; Liu et al., 2008; Deng et al., 2010; Hu et al., 2017, 2018a, 2018b; Cheng, 2019) have worked on constructing a three-pattern decomposition of global atmospheric circulation (3P-DGAC) since the end of the 1990s, based on the most important characteristics of global atmospheric circulation. The phenomena of Rossby waves in middle-high latitudes and Hadley and Walker circulations in low latitudes were first extended to the global general circulation, and the definitions of 3D horizontal, meridional, and zonal circulations were then quantified. The global atmospheric circulation was then decomposed into the sum of 3D horizontal circulation, meridional circulation, and zonal circulation; thus, the 3P-DGAC (Hu et al., 2018a) was established. Furthermore, combining the 3P-DGAC with the primitive equations of planetary-scale atmospheric motion, a new set of dynamical equations (Hu et al., 2018b) was established to directly describe the mechanisms of evolution of global large-scale horizontal circulation, meridional circulation, and zonal circulation. From a global perspective, the theory of 3P-DGAC unifies the atmospheric motions in the middle-high latitudes with those in low latitudes, which compensates for the deficiency of the partitioning of middle-high latitude atmospheric dynamics and low latitude atmospheric dynamics in the current study. It provides new ideas

and new theoretical tools to quantitatively study the relationship between atmospheric circulations in middle-high latitudes and those in low latitudes and the complex nonlinear interactions among horizontal, meridional, and zonal circulations, which is an original and innovative research achievement.

Based on a review of the traditional method of 2D circulation decomposition and its application in representation of the general circulation, this paper systematically introduces 3P-DGAC, and presents the theoretical advantages of the new method in representation of large-scale atmospheric circulations from a global perspective. By summarizing the 3P-DGAC, this study shows that the novel circulation decomposition model and its corresponding dynamical equations have potential application value in the study of the nonlinear source action mechanism of large-scale horizontal, meridional, and zonal circulations under the background of global warming.

2. Traditional 2D decomposition and its application in the representation of atmospheric circulation

For convenience in introducing 3P-DGAC, we need to briefly review the traditional 2D decomposition of vortex and divergent circulations and its application to the representation of atmospheric circulations in the middle-high latitudes and those in the low latitudes.

We know that the actual 3D atmospheric motion always satisfies the continuity equation in the p-coordinate system:

$$\nabla_p \cdot \mathbf{V} + \frac{\partial \omega}{\partial p} = 0, \tag{1}$$

where $\mathbf{V}(\lambda, \varphi, p) = u(\lambda, \varphi, p)\mathbf{i} + v(\lambda, \varphi, p)\mathbf{j}$ is horizontal velocity, $\omega(\lambda, \varphi, p)$ is vertical velocity, p is atmospheric pressure, and $\nabla_p = \mathbf{i}\frac{1}{a\cos\varphi}\frac{\partial}{\partial \lambda} + \mathbf{j}\frac{1}{a}\frac{\partial}{\partial \varphi}$ represents the gradient operator on the isobaric surface. Using the traditional decomposition of vortex and divergent circulations in 2D horizontal motion in hydrodynamics, the horizontal motion $\mathbf{V}$ along a given pressure surface p can always be decomposed into:

$$\mathbf{V}(\lambda, \varphi, p) = \mathbf{V}_{\text{div}}(\lambda, \varphi, p) + \mathbf{V}_{\text{rot}}(\lambda, \varphi, p), \tag{2}$$

where $\mathbf{V}_{\text{div}}$ and $\mathbf{V}_{\text{rot}}$ represent divergent wind (irrotational) and vortex wind (non-divergent) on the given isobaric surface, respectively. Eq. (2) also decomposes the continuity eq. (1) of the actual atmosphere into the following two parts:

$$\nabla_p \cdot \mathbf{V}_{\text{rot}} = 0, \tag{3}$$

$$\nabla_p \cdot \mathbf{V}_{\text{div}} + \frac{\partial \omega}{\partial p} = 0. \tag{4}$$

Here, eq. (3) represents the horizontal nondivergent vortex circulation, eq. (4) represents the vertical motion, and the actual atmospheric motion is always the superposition of these two parts.

2.1 Horizontal vortex circulation in middle-high latitudes

Because large-scale motions in the middle-high latitudes are mainly Rossby waves with vortex properties, and their velocity fields are quasi-horizontal and non-divergent, if the velocity components $\mathbf{V}_{\text{div}}$ and ω causing the vertical motion can be ignored, then the large-scale atmospheric motion in the middle-high latitudes is in the form of a horizontal vortex:

$$\mathbf{V}_{\text{rot}} = u_{\text{rot}}\mathbf{i} + v_{\text{rot}}\mathbf{j}, \tag{5}$$

which satisfies the continuity eq. (3), that is:

$$\frac{1}{a\cos\varphi}\frac{\partial u_{\text{rot}}}{\partial \lambda} + \frac{1}{a\cos\varphi}\frac{\partial v_{\text{rot}}\cos\varphi}{\partial \varphi} = 0. \tag{6}$$

According to the decomposition process of 2D vortex circulation and divergent circulation, if the vertical vorticity ζ_p of the atmosphere on the p isobaric surface is given, eq. (6) ensures that $\mathbf{V}_{\text{rot}}$ can be expressed as follows through the stream function ψ_{R}:

$$u_{\text{rot}} = -\frac{1}{a}\frac{\partial \psi_{\text{R}}}{\partial \varphi},\ v_{\text{rot}} = \frac{1}{a\cos\varphi}\frac{\partial \psi_{\text{R}}}{\partial \lambda}, \tag{7}$$

where ψ_{R} satisfies:

$$\Delta_2 \psi_{\text{R}} = \zeta_p. \tag{8}$$

Eqs. (7) and (8) show that if the influence of vertical motion is ignored, the motions in the middle-high latitudes on the isobaric surface can be equivalently expressed by a stream function ψ_{R}, which is the main reason why the image of ψ_{R} and the vertical vorticity equation are usually used to represent the evolution of Rossby waves in the middle-high latitudes.

Without considering the influence of vertical motion, the introduction of a stream function makes it more convenient to describe the main characteristics of large-scale horizontal vortex circulation in the middle-high latitudes. However because the vertical motion corresponding to the actual atmospheric convergence/divergence is often an essential factor in the occurrence and development of weather phenomena, it is necessary to generalize the quantitative description of vertical circulation in low latitudes to that in the middle-high latitudes in order to fully describe the real circulation system in middle-high latitudes.

2.2 Hadley and Walker circulations at low latitudes

In the tropics, owing to the vigorous development of vertical motion, the eddy component in the horizontal velocity field is often ignored, and atmospheric motion is simplified into a vertical circulation form meeting the continuity eq. (4) (Schwendike et al., 2014, 2015). For Hadley circulation at

low latitudes along the meridional direction, continuity eq. (4) is often used as the global zonal average (Wu, 1988; Hartmann, 1994; Trenberth and Caron, 2001):

$$\frac{1}{a\cos\varphi}\frac{\partial[v_{\mathrm{div}}]\cos\varphi}{\partial\varphi}+\frac{\partial[\omega]}{\partial p}=0, \tag{9}$$

where $[v_{\mathrm{div}}]=\frac{1}{2\pi}\int_0^{2\pi}v_{\mathrm{div}}\mathrm{d}\lambda$ and $[\omega]=\frac{1}{2\pi}\int_0^{2\pi}\omega\mathrm{d}\lambda$ represent the global zonal mean of v_{div} and ω, respectively. To describe Hadley circulation with mass flow, we rewrite eq. (9) as follows:

$$\frac{2\pi a}{g}\frac{\partial[v_{\mathrm{div}}]\cos\varphi}{\partial\varphi}+\frac{2\pi a^2\cos\varphi}{g}\frac{\partial[\omega]}{\partial p}=0. \tag{10}$$

Eq. (10) ensures that we can use the 2D mass stream function ψ_{H} to express the velocity fields $[v_{\mathrm{div}}]$ and $[\omega]$ of Hadley circulation as

$$[v_{\mathrm{div}}]=\frac{\mathrm{g}}{2\pi a\cos\varphi}\frac{\partial\psi_{\mathrm{H}}}{\partial p},\ [\omega]=-\frac{\mathrm{g}}{2\pi a^2\cos\varphi}\frac{\partial\psi_{\mathrm{H}}}{\partial\varphi}, \tag{11}$$

where ψ_{H} has the expression:

$$\psi_{\mathrm{H}}=\frac{2\pi a\cos\varphi}{\mathrm{g}}\int_0^p[v_{\mathrm{div}}]\mathrm{d}p, \tag{12}$$

or:

$$\psi_{\mathrm{H}}=-\frac{2\pi a^2}{\mathrm{g}}\int_{-\frac{\pi}{2}}^{\varphi}\cos\varphi[\omega]\mathrm{d}\varphi. \tag{13}$$

Because vertical velocity is not a direct observation variable, the mass stream function of Hadley circulation is usually calculated by eq. (12).

Similarly, to use the mass stream function to express the zonal vertical circulation, we often multiply the continuity eq. (4) by $\cos\varphi$, and then make the global meridional average to obtain:

$$\frac{1}{a}\frac{\partial<u_{\mathrm{div}}>}{\partial\lambda}+\frac{\partial<\omega\cos\varphi>}{\partial p}=0, \tag{14}$$

where $<u_{\mathrm{div}}>=\frac{1}{\pi}\int_{-\frac{\pi}{2}}^{\frac{\pi}{2}}u_{\mathrm{div}}\mathrm{d}\varphi$ and $<\omega\cos\varphi>=\frac{1}{\pi}\int_{-\frac{\pi}{2}}^{\frac{\pi}{2}}\cos\varphi\omega\mathrm{d}\varphi$ represent the global meridional average of u_{div} and $\omega\cos\varphi$, respectively. Further, we rewrite eq. (14) into:

$$\frac{\pi a}{\mathrm{g}}\frac{\partial<u_{\mathrm{div}}>}{\partial\lambda}+\frac{\pi a^2}{\mathrm{g}}\frac{\partial<\omega\cos\varphi>}{\partial p}=0. \tag{15}$$

Eq. (15) determines the relationship between the velocity field of the zonal vertical circulation and the mass stream function ψ_{W} as follows:

$$<u_{\mathrm{div}}>=\frac{\mathrm{g}}{\pi a}\frac{\partial\psi_{\mathrm{W}}}{\partial p},<\omega\cos\varphi>=-\frac{\mathrm{g}}{\pi a^2}\frac{\partial\psi_{\mathrm{W}}}{\partial\lambda}, \tag{16}$$

and ψ_W can be expressed as:

$$\psi_{\mathrm{W}}=\frac{\pi a}{\mathrm{g}}\int_0^p<u_{\mathrm{div}}>\mathrm{d}p, \tag{17}$$

or

$$\psi_{\mathrm{W}}=-\frac{\pi a^2}{\mathrm{g}}\int_0^{\lambda}<\omega\cos\varphi>\mathrm{d}\lambda. \tag{18}$$

Similarly, eq. (17) is often used to calculate the mass stream function of zonal vertical circulation.

Because the Walker circulation in the tropical Pacific region is the most influential large-scale vertical zonal circulation in the globe, to express it quantitatively, the mass stream function of Walker circulation is calculated using the meridional average $<u_{\mathrm{div}}>_{5^\circ\mathrm{S}}^{5^\circ\mathrm{N}}$ or $<u_{\mathrm{div}}>_{10^\circ\mathrm{S}}^{10^\circ\mathrm{N}}$ at low latitudes instead of the global meridional average $<u_{\mathrm{div}}>$ in eq. (17).

With respect to actual atmospheric circulations in low latitudes, in addition to the vertical overturning meridional and zonal circulations, there are also large horizontal vortex systems in the South Asia high, the West Pacific subtropical high, and other continents and oceans. Therefore, it is necessary to extend the description of horizontal vortex circulations in the middle-high latitudes to low latitudes.

3. Three-pattern decomposition of global atmospheric circulation

The traditional 2D circulation decomposition method has potential deficiencies in the representation of atmospheric circulation (Section 2). For instance, we often ignore the influences of the vertical motion in middle-high latitudes by using only the component part eq. (3) of the continuity equation. Similarly, we ignore the influence of the horizontal vortex motion in low latitudes by using only the component part eq. (4) of the continuity equation, which leads to the fact that the traditional 2D method cannot describe the global atmospheric circulation. At the same time, the 2D method artificially ignores the significant components of the general circulation, which has theoretical deficiencies. For example, if the vertical motion component is ignored in the middle-high latitudes, the occurrence, development, and extinction of the atmospheric system will not be fully demonstrated. Similarly, ignoring the horizontal circulation component in low latitudes results in misrepresentation of the complicated interactions between the middle-high and low latitude circulations. The 3P-DGAC is just a theory to solve the problem of a unified description of global atmospheric circulation.

For convenience in representing the 3D vortex vector in the right-hand spiral coordinate system, and without loss of generality, the spherical σ coordinate system is used in the 3P-DGAC (Hu et al., 2018a). Namely, we have:

$$u'=\frac{u}{a},v'=\frac{v}{a},\dot{\sigma}=\frac{\omega}{P_s},\sigma=\frac{p}{P_s}, \tag{19}$$

where P_s=1000 hPa denotes the sea level pressure, θ is co-latitude, and $(u',v',\dot{\sigma})$ and (u,v,ω) denote the three velocity components in the spherical σ coordinate system and spherical p coordinate system, respectively; thus, we can also use:

$$\begin{aligned}&\mathbf{V}'(\lambda,\theta,\sigma)\\&=u'(\lambda,\theta,\sigma)\mathbf{i}+v'(\lambda,\theta,\sigma)\mathbf{j}+\dot{\sigma}(\lambda,\theta,\sigma)\mathbf{k},\end{aligned} \tag{20}$$

to represent the 3D velocity field of the actual atmosphere. If we use latitude φ to replace the colatitude θ and insert eq. (19) into eq. (1), the continuity equation of the actual atmosphere can be rewritten as the following in the spherical σ coordinate system:

$$\frac{1}{\sin\theta}\frac{\partial u'}{\partial\lambda}+\frac{1}{\sin\theta}\frac{\partial(\sin\theta v')}{\partial\theta}+\frac{\partial\dot{\sigma}}{\partial\sigma}=0. \tag{21}$$

The 3P-DGAC introduced in this section is justly based on the continuity eq. (21). We first provide the definitions of 3D horizontal circulation, meridional circulation, and zonal circulation, and then introduce the 3P-DGAC.

3.1 Global horizontal, meridional, and zonal circulations

To accurately and quantitatively describe the 3D motion law of the actual atmosphere, we need to introduce vertical circulation to the representation of the middle-high latitude circulation, and introduce the horizontal vortex circulation in the representation of the low latitude circulation (Section 2). This means that we must extend the quantitative description of Hadley and Walker circulations in the low latitudes to the middle-high latitudes, and extend the description of horizontal vortex circulation in the middle-high latitudes to low latitudes. Thus, we have the definitions of global horizontal circulation, meridional circulation, and zonal circulation.

First, considering the characteristics of the horizontal Rossby wave in the middle-high latitudes introduced in Section 2.1, we define the velocity field of global horizontal circulation as follows (Hu et al., 2018a):

$$\mathbf{V}'_{\mathrm{R}}(\lambda,\theta,\sigma)=u'_{\mathrm{R}}(\lambda,\theta,\sigma)\mathbf{i}+v'_{\mathrm{R}}(\lambda,\theta,\sigma)\mathbf{j}, \tag{22}$$

which satisfies the following continuity equation:

$$\frac{1}{\sin\theta}\frac{\partial u'_{\mathrm{R}}}{\partial\lambda}+\frac{1}{\sin\theta}\frac{\partial\left(\sin\theta v'_{\mathrm{R}}\right)}{\partial\theta}=0. \tag{23}$$

The vertical velocity of horizontal circulation $\mathbf{V}'_{\mathrm{R}}$ is zero, but the variation of horizontal velocity with height shows that $\mathbf{V}'_{\mathrm{R}}$ can describe the baroclinic characteristics of horizontal motion in the vertical direction. By introducing the stream function $R(\lambda,\theta,\sigma)$, eq. (23) ensures that the components u'_{R} and v'_{R} of $\mathbf{V}'_{\mathrm{R}}$ can be expressed as

$$u'_{\mathrm{R}}=-\frac{\partial R}{\partial\theta},v'_{\mathrm{R}}=\frac{1}{\sin\theta}\frac{\partial R}{\partial\lambda}. \tag{24}$$

Because $\mathbf{V}'_{\mathrm{R}}$ is the 3D spatial horizontal circulation, its components u'_{R} and v'_{R} are all related to σ. Unlike the 2D case on a fixed isobaric surface, eq. (23) cannot guarantee the uniqueness of the stream function $R(\lambda,\theta,\sigma)$ defined by eq. (24). For example, for any given σ-related differentiable function $f(\sigma)$, the function $R(\lambda,\theta,\sigma)+f(\sigma)$ still satisfies eq. (24). Therefore, we need to find a new way to solve the uniqueness problem of the 3D stream function $R(\lambda,\theta,\sigma)$.

Similarly, according to the characteristics of Hadley and Walker circulations in the low latitudes (Section 2.2), we define the velocity fields of global meridional circulation $\mathbf{V}'_{\mathrm{H}}$ and zonal circulation $\mathbf{V}'_{\mathrm{W}}$ using the following formulae (Hu et al., 2018a):

$$\mathbf{V}'_{\mathrm{H}}(\lambda,\theta,\sigma)=v'_{\mathrm{H}}(\lambda,\theta,\sigma)\mathbf{j}+\dot{\sigma}_{\mathrm{H}}(\lambda,\theta,\sigma)\mathbf{k}, \tag{25}$$

$$\mathbf{V}'_{\mathrm{W}}(\lambda,\theta,\sigma)=u'_{\mathrm{W}}(\lambda,\theta,\sigma)\mathbf{i}+\dot{\sigma}_{\mathrm{W}}(\lambda,\theta,\sigma)\mathbf{k}, \tag{26}$$

which satisfy the following continuity equations:

$$\frac{1}{\sin\theta}\frac{\partial\left(\sin\theta v'_{\mathrm{H}}\right)}{\partial\theta}+\frac{\partial\dot{\sigma}_{\mathrm{H}}}{\partial\sigma}=0, \tag{27}$$

$$\frac{1}{\sin\theta}\frac{\partial u'_{\mathrm{W}}}{\partial\lambda}+\frac{\partial\dot{\sigma}_{\mathrm{W}}}{\partial\sigma}=0. \tag{28}$$

Similarly, eqs. (27) and (28) ensure that the components of $\mathbf{V}'_{\mathrm{H}}$ and $\mathbf{V}'_{\mathrm{W}}$ can be represented by stream functions, $H(\lambda,\theta,\sigma)$ and $W(\lambda,\theta,\sigma)$, respectively, as follows:

$$v'_{\mathrm{H}}=-\frac{\partial H}{\partial\sigma},\ \dot{\sigma}_{\mathrm{H}}=\frac{1}{\sin\theta}\frac{\partial(\sin\theta H)}{\partial\theta}, \tag{29}$$

$$u'_{\mathrm{W}}=\frac{\partial W}{\partial\sigma},\ \dot{\sigma}_{\mathrm{W}}=-\frac{1}{\sin\theta}\frac{\partial W}{\partial\lambda}. \tag{30}$$

For the same reason, $H(\lambda,\theta,\sigma)$ and $W(\lambda,\theta,\sigma)$ cannot be uniquely determined by eqs. (27) and (28). We will resolve this issue in the next section.

Eq. (25) shows that although the meridional circulation represented by $\mathbf{V}'_{\mathrm{H}}$ only moves in the meridional plane, it has spatially varying characteristics in the zonal direction. Similarly, eq. (26) shows that the zonal circulation represented by $\mathbf{V}'_{\mathrm{W}}$ has the characteristics of spatial variation in the meridional direction. These characteristics indicate that the actual atmospheric circulation is not only a 3D horizontal circulation, meridional circulation or zonal circulation, but a superposition of all three.

Analyzing the above descriptions and definitions of eqs. (22)–(30), we find that the definitions of global horizontal circulation, meridional circulation, and zonal circulation are irrelevant to the temporal and spatial scales of the actual circulation system. Therefore, the concepts of global horizontal circulation, meridional circulation, and zonal circulation make it possible to quantitatively study the evolution of 3D structural characteristics of atmospheric circulation at different temporal and spatial scales.

3.2 Three-pattern decomposition of global atmospheric circulation

As discussed in the previous section, global atmospheric circulation should be considered in its entirety. The atmospheric circulation in the middle-high latitudes not only has a horizontal vortex component, but also includes the vertical motion corresponding to the horizontal vortex. Similarly, the atmospheric circulation in low latitudes has not only the

vertical component, but also the horizontal vortex related to the vertical motion. Therefore, from a global perspective, the actual atmospheric circulation $\mathbf{V}'$ can be expressed as the superposition of horizontal circulation $\mathbf{V}'_{\mathrm{R}}$, meridional circulation $\mathbf{V}'_{\mathrm{H}}$, and zonal circulation $\mathbf{V}'_{\mathrm{W}}$ as follows:

$$\mathbf{V}' = \mathbf{V}'_{\mathrm{H}} + \mathbf{V}'_{\mathrm{W}} + \mathbf{V}'_{\mathrm{R}}, \tag{31}$$

with its components expressed as

$$\begin{cases} u' = u'_{\mathrm{W}} + u'_{\mathrm{R}} = \dfrac{\partial W}{\partial \sigma} - \dfrac{\partial R}{\partial \theta}, \\ v' = v'_{\mathrm{R}} + v'_{\mathrm{H}} = \dfrac{1}{\sin\theta}\dfrac{\partial R}{\partial \lambda} - \dfrac{\partial H}{\partial \sigma}, \\ \dot{\sigma} = \dot{\sigma}_{\mathrm{H}} + \dot{\sigma}_{\mathrm{W}} == \dfrac{1}{\sin\theta}\dfrac{\partial(\sin\theta H)}{\partial \theta} - \dfrac{1}{\sin\theta}\dfrac{\partial W}{\partial \lambda}. \end{cases} \tag{32}$$

According to the definitions of eqs. (23), (27), and (28), the superposition of $\mathbf{V}'$ in eq. (31) still satisfies continuity eq. (21). This shows that the decomposition $\mathbf{V}'_{\mathrm{R}}$, $\mathbf{V}'_{\mathrm{H}}$, and $\mathbf{V}'_{\mathrm{W}}$ of the real atmospheric circulation $\mathbf{V}'$ correspond to a decomposition (eqs. (23), (27), and (28)) of continuity eq. (21). If $\mathbf{V}'_{\mathrm{R}}$, $\mathbf{V}'_{\mathrm{H}}$ and $\mathbf{V}'_{\mathrm{W}}$ reduce to a given isobaric surface, the global zonal average plane and the global meridional average plane, respectively, eqs. (23), (27), and (28) are equal to eqs. (6), (9), and (14), respectively, which further shows that the horizontal circulation $\mathbf{V}'_{\mathrm{R}}$, meridional circulation $\mathbf{V}'_{\mathrm{H}}$, and zonal circulation $\mathbf{V}'_{\mathrm{W}}$ are the global generalizations of the traditional Rossby wave, Hadley circulation, and Walker circulation.

We call eq. (31) or eq. (32) the 3P-DGAC (Hu et al., 2018a). However, unlike the decomposition of 2D circulation (introduced in Section 1), since horizontal circulation $\mathbf{V}'_{\mathrm{R}}$, meridional circulation $\mathbf{V}'_{\mathrm{H}}$, and zonal circulation $\mathbf{V}'_{\mathrm{W}}$ have three spatial dimensions, we need the following restriction condition (Hu et al., 2018a):

$$\frac{1}{\sin\theta}\frac{\partial H}{\partial \lambda} + \frac{1}{\sin\theta}\frac{\partial(W\sin\theta)}{\partial \theta} + \frac{\partial R}{\partial \sigma} = 0, \tag{33}$$

to select the correct stream functions (H, W, and R). Eq. (33) guarantees not only the uniqueness of the stream functions (H, W, and R), but also the physical rationality of the 3P-DGAC. A more detailed discussion can be found in Theorem 2 of Hu et al. (2018a).

Combining eq. (33) with eq. (32), we have stream functions H, W, and R satisfy the following equations:

$$\Delta_3 R = \zeta, \tag{34}$$

$$\frac{\partial H}{\partial \sigma} = \frac{1}{\sin\theta}\frac{\partial R}{\partial \lambda} - v', \tag{35}$$

$$\frac{\partial W}{\partial \sigma} = \frac{\partial R}{\partial \theta} + u', \tag{36}$$

where $\zeta = \dfrac{1}{\sin\theta}\dfrac{\partial v'}{\partial \lambda} - \dfrac{1}{\sin\theta}\dfrac{\partial(u'\sin\theta)}{\partial \theta}$ represents the vertical vorticity of the entire atmospheric layer and $\Delta_3 = \dfrac{1}{\sin^2\theta}\dfrac{\partial^2}{\partial \lambda^2} + \dfrac{1}{\sin\theta}\dfrac{\partial}{\partial \theta}\left(\sin\theta\dfrac{\partial}{\partial \theta}\right) + \dfrac{\partial^2}{\partial \sigma^2}$ represents the 3D Laplacian in the spherical σ-coordinate system. By solving eqs. (34)–(36), we obtain the stream functions H, W, and R which leads to the 3P-DGAC.

3.3 Climatic evolution characteristics of global horizontal, meridional, and zonal circulations

To verify the rationality and correctness of the 3P-DGAC, we first analyzed the climatic characteristics of global horizontal, meridional, and zonal circulation and then introduce the climatic evolutions of Hadley and Walker circulations by using the results of 3P-DGAC based on the five reanalysis datasets (NCEP1, NCEP2, ERAI, JRA-55, and MERRA) in this section. By substituting the zonal wind u and meridional wind v of the five reanalysis datasets into eqs. (34)–(36), we obtain the stream functions H, W, and R. By calculating eqs. (24), (29), and (30), we have horizontal circulation $\mathbf{V}_{\mathrm{R}}$, meridional circulation $\mathbf{V}_{\mathrm{H}}$ and zonal circulation $\mathbf{V}_{\mathrm{W}}$ with their six velocity components (u_{R}, v_{R}, v_{H}, ω_{H}, u_{W}, and ω_{W}). It should be noted that the velocity field in the σ-coordinate system is transformed into the p-coordinate system by using the transformation relation (19). Therefore, the unit of horizontal velocities (u_{R}, u_{W},v_{R} and v_{H}) in this study is m s^{-1}, and the unit of vertical velocities (ω_{H} and ω_{W}) is Pa s^{-1}, while the stream functions H, W, and R still retain the unit of 10^{-6} s^{-1} in the σ-coordinate system.

3.3.1 Climatic characteristics

According to eq. (34), in the northern hemisphere, the positive region of the stream function R represents the negative vorticity, which corresponds to the anticyclonic high-pressure circulation system, and the negative region of R denotes the positive vorticity that corresponds to the cyclonic low-pressure circulation system; in the southern hemisphere, the reverse applies. Figure 1 shows the climatic characteristics of horizontal circulation in January and July. This indicates that there exist two circumpolar low-pressure systems around the north and the south poles, among which the isoline of the stream function R around the Arctic pole has clear wavelike distribution characteristics, while the isoline of the stream function around the Antarctic pole is relatively straight. There are three major troughs at the middle latitudes of the northern hemisphere in boreal winter, which are located on the east coast of the Asian continent, the east coast of the American continent, and the eastern part of Europe; the last of which is the weakest (Figure 1a). Figure 1b shows that the horizontal circulation in the lower troposphere in July is characterized by the following features. First, the great trough in eastern Europe at middle-high latitudes extends southward to the Arabian Peninsula and the vast area of the Indian subcontinent near 15°N. Second, in the Atlantic, the Pacific, and the equatorial western Indian Ocean near 30°N, the positive center of the stream function of horizontal

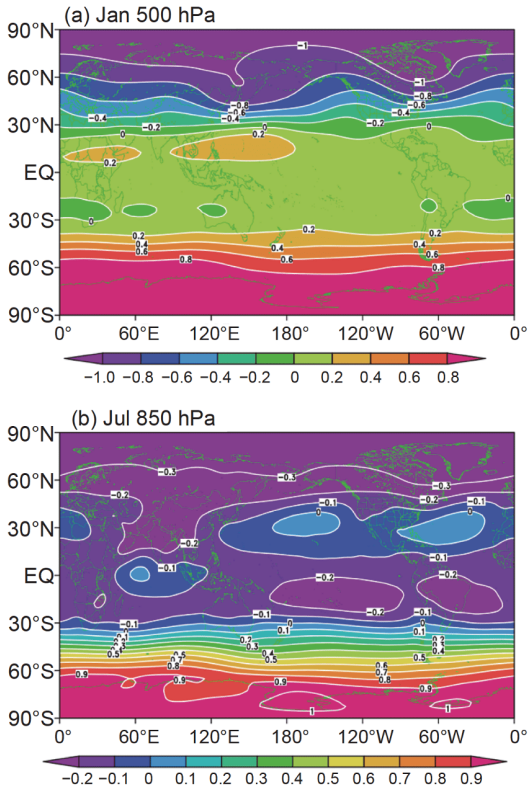

Figure 1 The climatological mean of stream function R (contour and shading; unit: 10^{-6} s^{-1}) in (a) January and (b) July (1948–2011). Cited from Hu et al. (2018a).

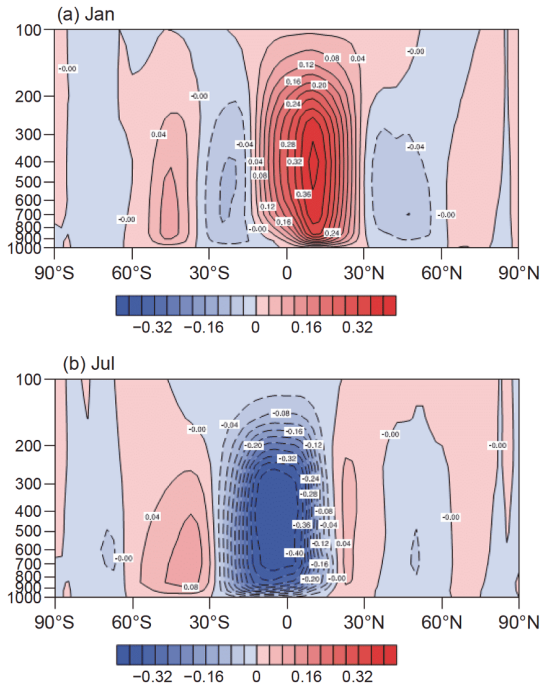

Figure 2 Climatic characteristics of global zonal-mean stream function H of the meridional circulation in (a) January and (b) July (1948–2011) (contour and shading, unit: 10^{-6} s^{-1}).

circulation corresponds to an anticyclonic high-pressure system. Negative centers of the stream function of horizontal circulation in the Pacific Ocean and South American continent are apparent, which means that these regions are controlled by closed anticyclonic high-pressure systems. The above analysis reveals that the stream function of the horizontal circulation defined in this paper not only reflects the main characteristics of the large-scale horizontal circulation in the middle-high latitudes, but also describes the main characteristics of the large-scale horizontal circulation in the latitudes.

Figure 2 represents the climatic characteristics of the global zonally averaged meridional circulation in January and July, and Figure 3 shows its global distribution. In the northern hemisphere, the negative region of the stream function H represents the meridional circulation, ascending in the low latitudes and descending in the high latitudes, and the positive region of the stream function H represents the meridional circulation, ascending in high latitudes and descending in low latitudes. The reverse applies in the southern hemisphere. Figure 2 shows that the meridional circulation has three-cell characteristics in both the southern and northern hemispheres, that is, the traditional Hadley circulation, Ferrel circulation, and polar circulation. The position centers of these meridional circulations exhibit seasonal north-south movement, and the circulation intensities also have distinct seasonal characteristics (the figures in the transition season are omitted). For example, in January (boreal winter), Hadley circulation in the northern hemisphere is the strongest. It ascends in the tropics and descends in the subtropical regions of the northern hemisphere. The Hadley circulation in the southern hemisphere is weak, and its areal coverage is relatively small. However, the reverse applies in July (boreal summer). The Hadley circulation in the northern hemisphere is weak and its areal coverage reduces significantly, while the Hadley circulation in the southern hemisphere is strong and ascends north of the equator and descends in the subtropical area of the southern hemisphere. In the boreal winter, there are four strong meridional circulation centers south of 30°N (Figure 3a). They are located on continental Europe, the east coast of the Asian continent, the North American continent, and the North Atlantic, which shows that the meridional circulation has significant local characteristics. In addition to the opposite situation in the East Pacific, the winter meridional circulations in low latitudes are mainly in the form of Hadley circulation, ascending in low latitudes and descending in the high latitudes. In summer (Figure 3b), the meridional circulation in the northern hemisphere weakens and shifts northward. In the eastern Pacific, the reverse meridional circulation in winter changes into Hadley circulation in summer. This shows that the meridional circulation exhibits obvious seasonal conversions, not only in the low latitudes,

but also in the middle-high latitudes.

Compared with the zonally averaged results, Figure 3 is more representative of the global distribution of meridional circulation. A significant feature of Figures 2 and 3 is that the meridional circulation in winter is stronger and wider than that in summer, and there are several large closed centers around the globe. According to the different directions of the Hadley circulation, these closed centers present an interval distribution, which may be related to thermal differences between land and sea in the corresponding areas. The above analysis demonstrates that the stream function H defined in this study can better reflect the evolution of the local Hadley circulation, and can provide new data for further examination of the evolution of the local Hadley circulation. In addition, in recent years, Qian et al. (2015, 2016, 2017) proposed a new concept of a four-cell meridional circulation model in the northern and southern hemispheres by using the mass stream function to study global zonally-averaged meridional circulations. They concluded that the fourth meridional circulation in the Arctic region has an important impact on the weather and climate in middle-high latitudes of the northern hemisphere. We also find that the stream function H supports the same conclusion, that is, there exists a fourth polar meridional circulation in the global zonally-averaged H (Figure 2), which further verifies the accuracy and validity of the stream function H representing global meridional circulations.

Figure 4 represents the climatic characteristics of meridional-mean zonal circulation in January and July, and Figure 5 shows its global distribution. Negative values of the stream function W represent the zonal circulation ascending in the east and descending in the west of the eastern hemisphere (the Walker circulation), and positive values of the stream function W represent the zonal circulation ascending in the west and descending in the east of the Western Hemisphere (an anti-Walker circulation). Figure 4 shows that in the equatorial region, there are several zonal circulations throughout the year, the main structure of which is the upward movement on the warm ocean surface of Indonesia and the Western Pacific and the downward movement on the eastern and western sides. The zonal circulation that ascends in the West Pacific and descends in the East Pacific is often called Walker circulation, and the zonal circulation that ascends in the West Pacific and Indonesia and descends in the West Indian Ocean and Africa is an anti-Walker circulation. Figure 4 also shows that the zonal circulation in the equatorial region exhibits clear seasonal variations. In January, the Walker circulation across the equatorial Pacific is the strongest, the zonal circulation in South America, and the Atlantic are the second strongest, while the zonal circulation in Africa and the Indian Ocean are the weakest. In contrast, in July, the Walker circulation in the equatorial Pacific

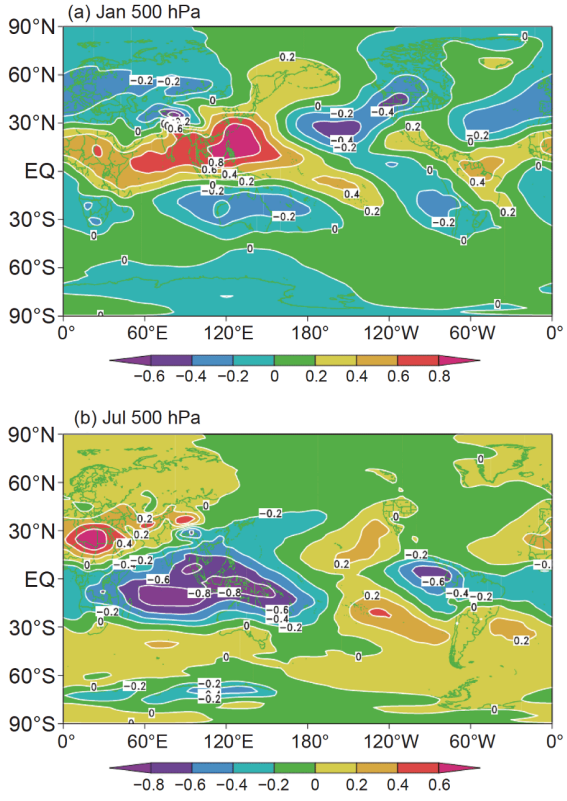

Figure 3 Global distribution characteristics (contour and shading, unit: 10^{-6} s^{-1}) of stream function H at 500 hPa in (a) January and (b) July (1948–2011). Cited from Hu et al. (2018a).

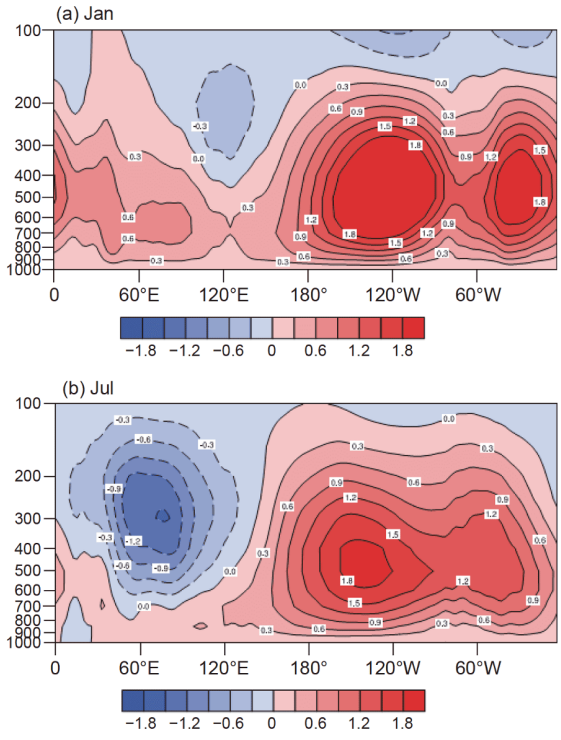

Figure 4 Climatic characteristics of meridional-mean stream function W of the zonal circulation between 10°S and 10°N (contour and shading, unit: 10^{-6} s^{-1}) in (a) January and (b) July (1948–2011).

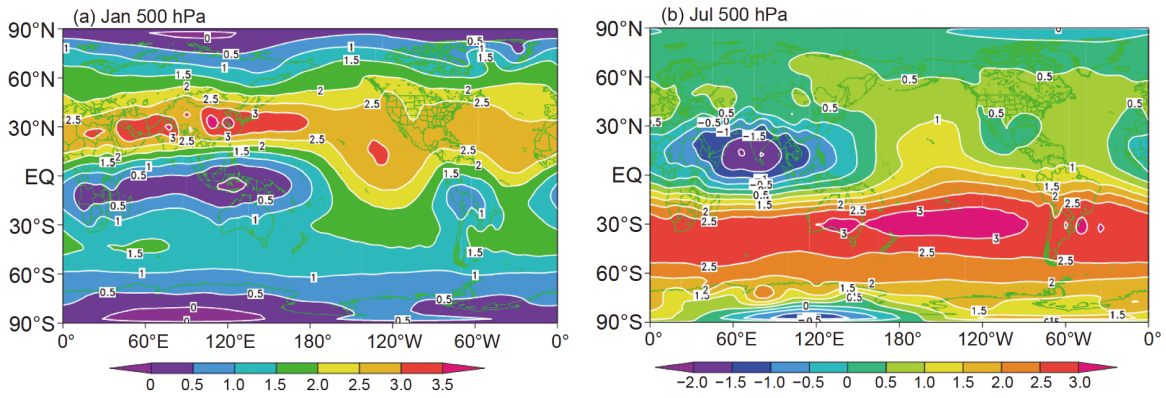

Figure 5 Global distribution characteristics (contour and shading, unit: 10^{-6} s^{-1}) of stream function W at 500 hPa in (a) January and (b) July (1948–2011). Cited from Hu et al. (2018a).

weakens, the anti-Walker circulation over Africa and the Indian Ocean strengthens and the circulation center shifts eastward.

Figure 5 shows that in January, the zonal circulation is mainly distributed in the low latitudes between 30°S and 30°N. In addition to the Walker-pattern circulation in the eastern equatorial Pacific, there are two anti-Walker-pattern circulations from the equator to 30°S. One is zonal circulation across the whole eastern hemisphere, with its center located over Indonesia, the Indian Ocean, and the African continent, and the other is the zonal circulation with its center located over the South American continent. The region between 15°N and 30°N is controlled by Walker-pattern circulations, and one of the strongest circulation centers is located on the east coast of China. In July, the zonal circulation in the equatorial region and the north of the equatorial region shifts northward, and the Walker-pattern circulation in the equatorial Pacific region expand its range, while the anti-Walker-pattern circulation in Indonesia and the Indian Ocean region narrows its areal extent, with its intensity strengthening. Similarly, compared with the meridional-mean results, Figure 5 is more representative of the global distribution of the zonal circulation.

3.3.2 Climatic evolution of Hadley and Walker circulations

As we know from the previous section, Hadley and Walker circulations in the low latitudes are the most powerful meridional and zonal circulations, with the widest spatial range, which play a very important role in the abnormal evolution of global climate. In this section, we introduce the climatic evolution of Hadley and Walker circulations based on the 3P-DGAC.

Figure 6 shows long-term changes and climatological distributions of the global zonal-mean stream function H of the meridional circulation calculated using five reanalysis datasets (NCEP1, NCEP2, ERAI, JRA-55, and MERRA) from 1979 to 2015. Since the Hadley circulation in the northern (southern) hemisphere corresponds to a positive (negative) value of the stream function H, the positive (negative) trend of the stream function indicates an enhancement of the Hadley circulation in the northern (southern) hemisphere, and vice versa. Figure 6 shows that in recent decades, the Hadley circulation in the northern hemisphere has significantly strengthened in winter and spring, while in the southern hemisphere it has intensified in all seasons, and it is strongest in autumn. In the subtropical region, the poleward edge of Hadley circulation can be represented by the latitude where the stream function of the meridional circulation at 500 hPa is zero (Hu and Fu, 2007). There is an obvious negative (positive) trend on both sides of the poleward edges of Hadley circulation in winter and spring (summer and autumn) of the southern (northern) hemisphere, which indicates that the Hadley circulation has exhibited a clear poleward movement in recent decades (Figure 6).

To quantitatively describe the evolution of the intensity and poleward edge of Hadley circulation in recent decades, referring to the research of Oort and Yienger (1996), Cheng et al. (2018a, 2018b) defined the intensity index of Hadley circulation by computing the average value of the stream function H over the latitude-height cross section around the circulation center from 850 to 300 hPa. They also defined the poleward edge index of the Hadley circulation by determining the average latitude of the zero value of the vertical mean (850 to 300 hPa) stream function H in a subtropical area. The standardized time series of the Hadley circulation intensity index in from 1979 to 2015 from five reanalysis datasets is shown in Figure 7. Figure 8 shows the evolution of the poleward edge of Hadley circulation in each season. In boreal winter and spring, and all seasons in the southern hemisphere, Hadley circulation is significantly enhanced, and there are significant trends in poleward expansion in the summer and autumn in both hemispheres (Figure 8). The Hadley circulation in the Northern Hemisphere exhibits a 0.99° decade^{-1} (or 3.7° in 37 years) poleward expansion in MERRA and 0.38° decade^{-1} (or 1.4° in

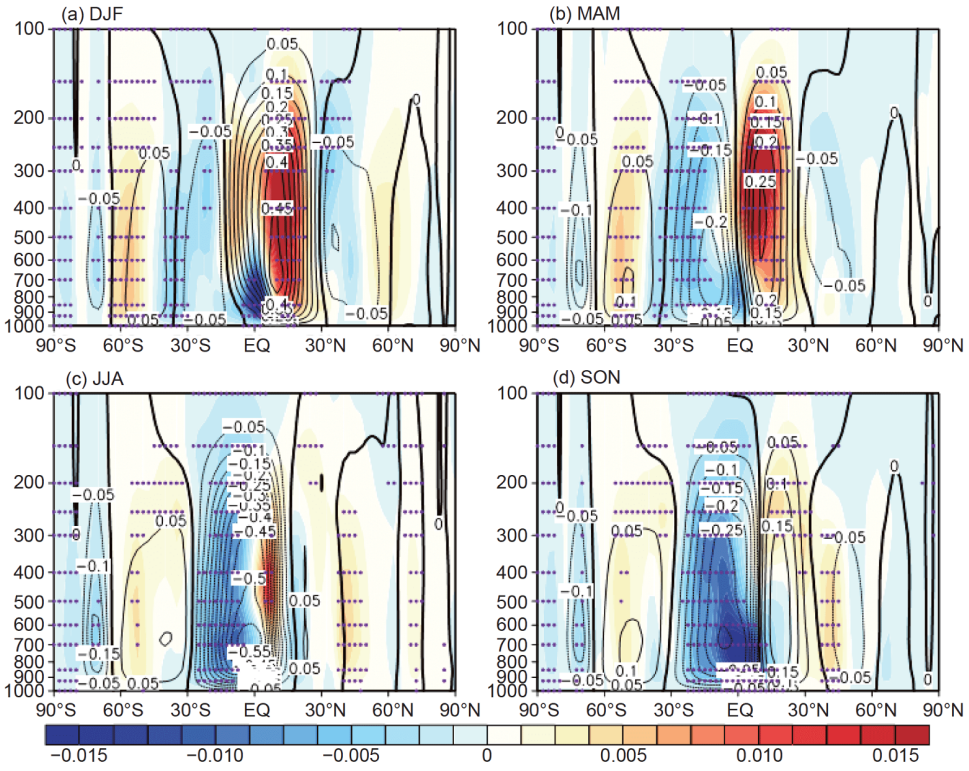

Figure 6 Linear trends (shading, unit: 10^{-6} s^{-1} $decade^{-1}$) of global zonally averaged stream function H in (a) winter, (b) spring, (c) summer, and (d) autumn in the Northern Hemisphere from 1979 to 2015, with the dotted trends that are significant (p<0.05). The contours represent the climatic state of the global zonally averaged stream function H. Cited from Cheng et al. (2018a).

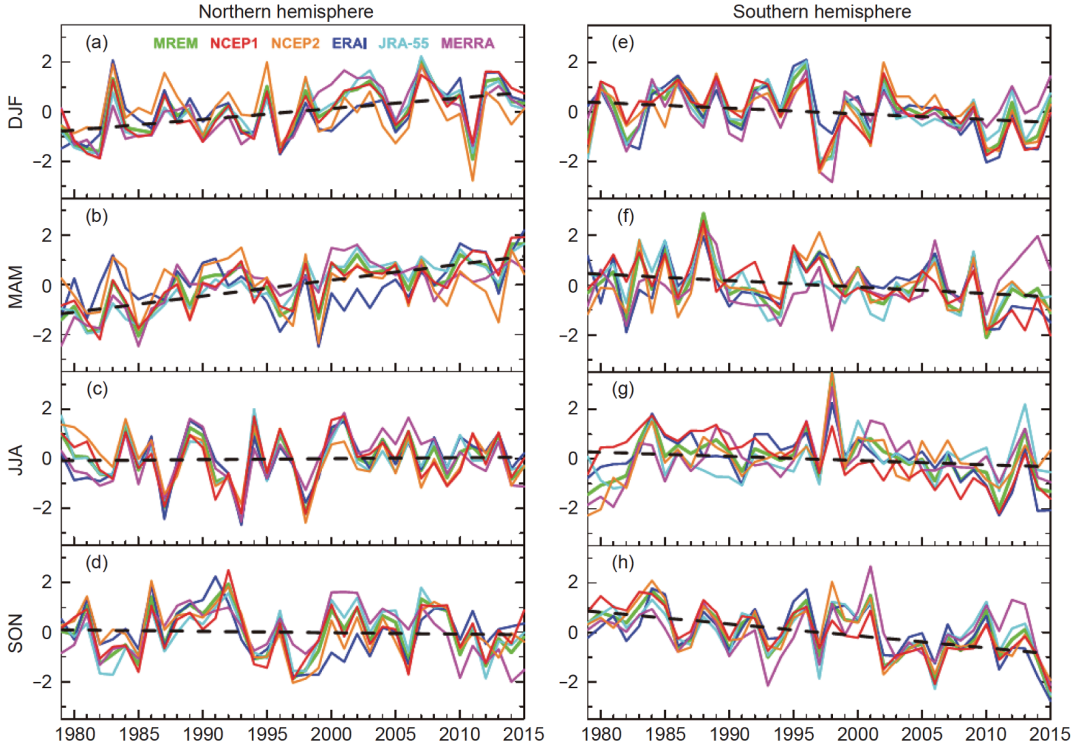

Figure 7 Normalized time series of intensity indices of Hadley circulation in (a) winter, (b) spring, (c) summer, and (d) autumn in the Northern Hemisphere from 1979 to 2015. Different colored lines represent different reanalysis datasets. The black dashed line in each plot represents the average linear trend of the five reanalysis datasets. (e)–(h) are the same as (a)–(d), but for Hadley circulation in the southern hemisphere. Cited from Cheng et al. (2018a).

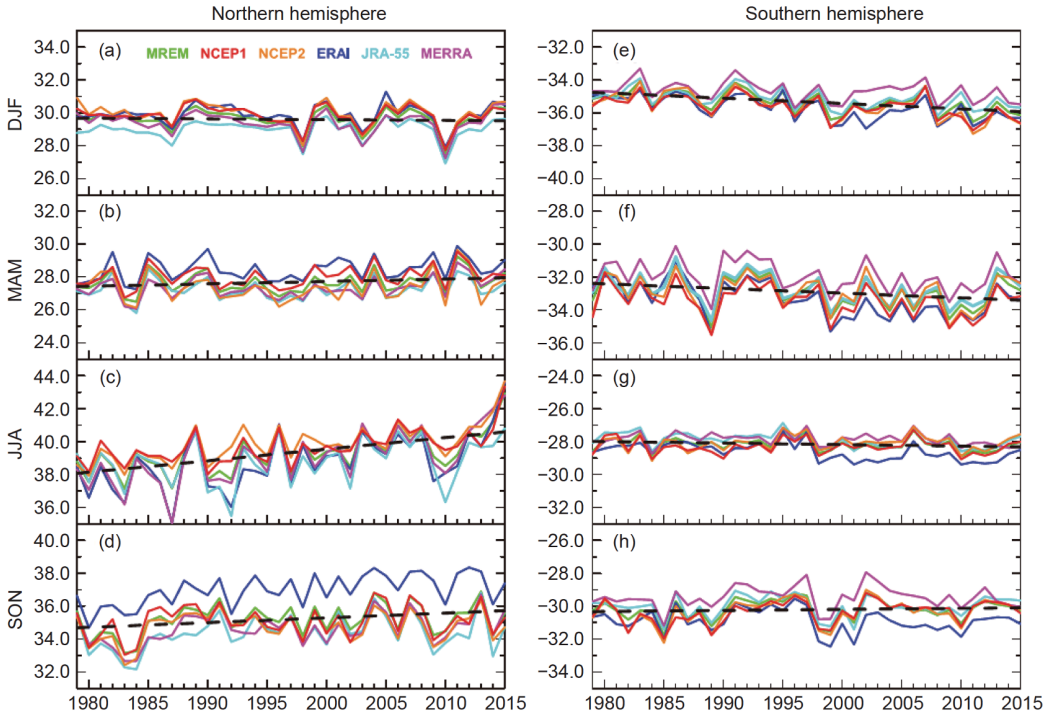

Figure 8 Same as Figure 7, but for the poleward edges of Hadley circulation. Cited from Cheng et al. (2018a).

37 years) in JRA-55 during boreal summer(Figure 9). Similarly, the result in ERAI is 0.5° decade^{-1} (or 1.9° in 37 years) and 0.16° decade^{-1} (or 0.6° in 37 years) in NCEP2 during the boreal autumn. In the Southern Hemisphere, the poleward shift is 0.20° per decade (or 0.7° in 37 years) in MERRA, and 0.44° per decade (or 1.6° in 37 years) in NCEP2 during the boreal winter. In ERAI the shift is 0.52° per decade (or 1.9° in 37 years) and 0.15° per decade (or 0.6° in 37 years) in NCEP2 during the boreal spring (Figure 9). Although the results in the five reanalysis datasets differ, their trends were consistent, which again verifies the previous conclusions.

Similarly, the stream function W of the zonal circulation defined by the 3P-DGAC can describe the inter-decadal evolution of Walker circulation in recent decades very well (Hou et al., 2018). During the decades 1961–1974 and 1977–1997, the Walker circulation in the equatorial Pacific weakened and shifted westward, while in the decades 1977–1997 and 1999–2012, it significantly strengthened and shifted eastward (Figure 10). Except for minor differences, the trend of Walker circulation in each month (Figure 11) is almost consistent with the annual average. For example, between 1961–1974 and 1977–1997, the Walker circulation in boreal autumn shows the largest weakening trend, while between 1977–1997 and 1999–2012, the Walker circulation in boreal spring clearly strengthened.

Good correspondence between the inter-decadal evolution of Walker circulation and the 3D temperature gradient was

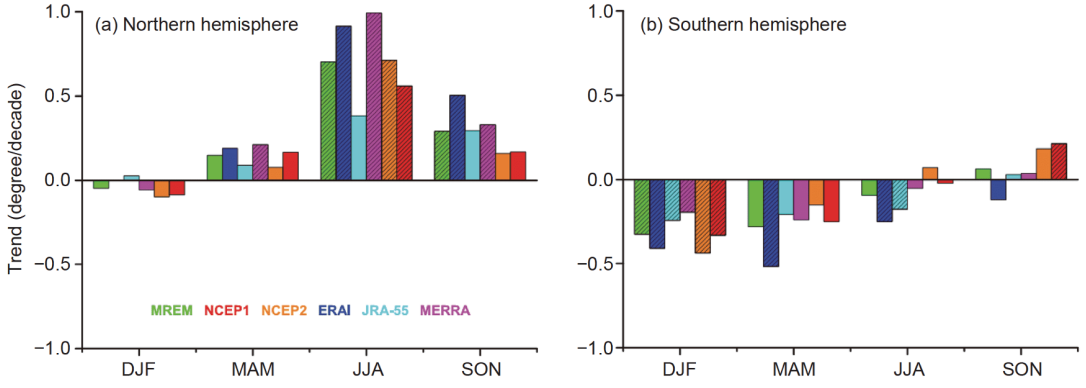

Figure 9 Linear trends of the poleward edges of Hadley circulation in different seasons in the northern hemisphere (a) and the southern hemisphere (b) between 1979 and 2015. The oblique lines represent trends that are significant (p<0.05). Cited from Cheng et al. (2018a).

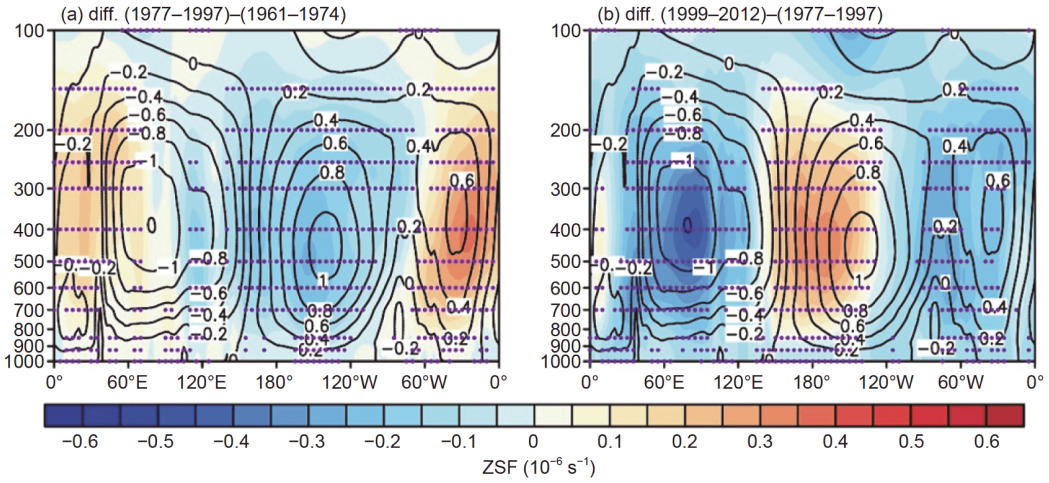

Figure 10 Differences (shading) of annual mean stream function W of zonal circulation in the region (5°S–5°N) between (a) 1961–1974 and 1977–1997 and (b) the 1977–1997 and 1999–2012. The dots indicate that the differences are significant (p<0.05). The contours represent the climatic state (1961–2012) of meridionally averaged stream function W between 5°S and 5°N. Cited from Hou et al. (2018).

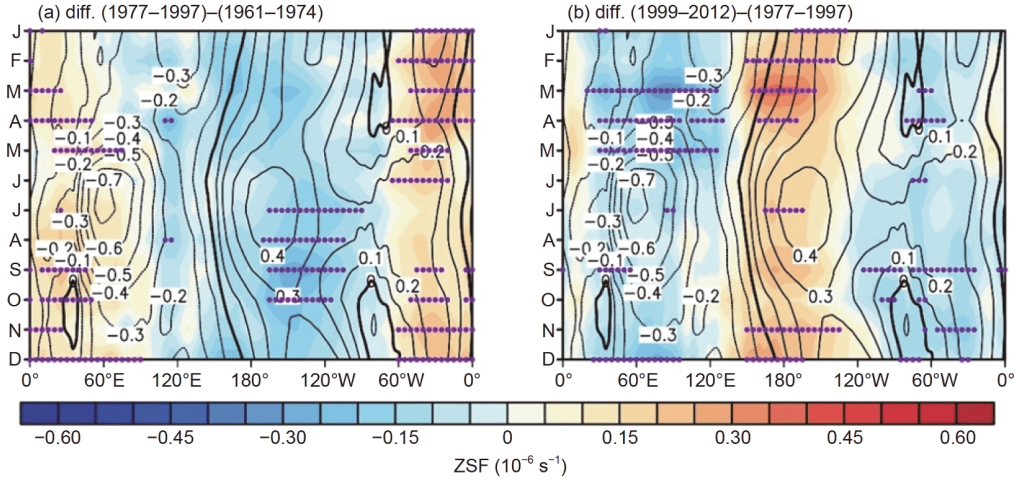

Figure 11 Same as Figure 10, but demonstrates the differences (shading) of vertically averaged stream function W in the region (5°S–5°N) for each month. Cited from Hou et al. (2018).

demonstrated in the four time periods discussed above (Hou et al., 2018). Therefore, Hou et al. (2018) proposed a new definition of the Walker circulation intensity index based on the 3D temperature field as follows:

$$T_{\text{index}} = TW_{1000\ \text{hPa}} + TW_{500\ \text{hPa}} + TE_{100\ \text{hPa}} - (TE_{1000\ \text{hPa}} + TE_{500\ \text{hPa}} + TW_{100\ \text{hPa}}), \quad (37)$$

where T is air temperature, TW is the averaged air temperature over the region (5°S–5°N, 80°W–160°W), TE is the averaged air temperature over the region (5°S–5°N, 80°E–160°E), and the subscript represents different pressure layers. In previous studies, the average sea level pressure (SLP) gradient between the regions (5°S–5°N, 80°W–160°W) and (5°S–5°N, 80°E–160°E) is commonly used to define the Walker circulation intensity index. Similar to the Hadley circulation, the averaged value of the stream function W in the region of the circulation center (5°S–5°N, 120°W–160°W, 300–600 hPa) is also used to represent the Walker circulation intensity. Inter-annual and inter-decadal evolution of Walker circulation represented by these three indices is consistent, providing confirmation that the stream function W reflects the climatic evolution of Walker circulation (Figure 12).

4. Three-pattern decomposition of global atmospheric circulation: physical decomposition of vertical vorticity and vertical velocity

In this section, we explain the advantages of 3P-DGAC in describing global atmospheric circulations with respect to the decomposition of vertical vorticity and vertical velocity.

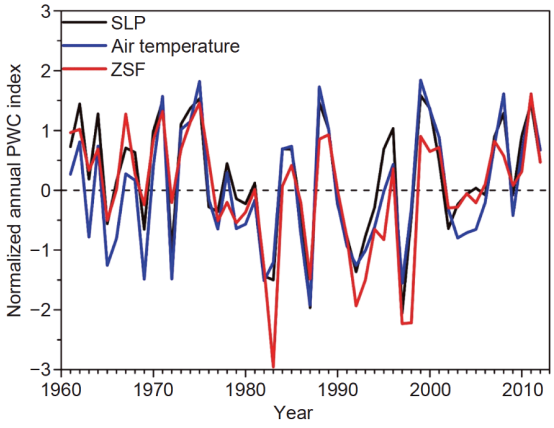

Figure 12 Normalized time series of annual averaged intensity indices of Walker circulation (1961–2012), SLP represents sea level pressure index (black line), and air temperature index is defined by eq. (37) (blue line), ZSF represents the stream function W index (red line). Cited from Hou et al. (2018).

4.1 Decomposition of the vertical vorticity

On a given isobaric surface, the horizontal vortex circulation $\mathbf{V}_{\mathrm{rot}}$ obtained by the traditional 2D circulation decomposition method satisfies the following 2D Poisson equation:

$$\Delta_2\psi_{\mathrm{R}} = \zeta_p, \tag{38}$$

here, ζ_p is the actual vertical vorticity ζ on a given pressure surface. Eq. (38) shows that the traditional 2D method needs to limit the motion to a certain isobaric surface. Therefore, the horizontal vortex circulation $\mathbf{V}_{\mathrm{rot}}$ corresponds to all the vertical vorticity of the actual atmosphere, while the vertical vorticity caused by the horizontal convergent/divergent motion cannot be expressed by the 2D circulation decomposition method.

The horizontal circulation obtained from the 3P-DGAC (Section 3.2), however, satisfies the following 3D Poisson equation:

$$\Delta_3 R = \Delta_2 R + \frac{\partial^2 R}{\partial \sigma^2} = \zeta, \tag{39}$$

$\Delta_2 R = \frac{1}{\sin\theta}\frac{\partial v'_{\mathrm{R}}}{\partial \lambda} - \frac{1}{\sin\theta}\frac{\partial u'_{\mathrm{R}}\sin\theta}{\partial \theta}$ can be computed by eq. (24), which represents the vertical vorticity of the 3D horizontal circulation $\mathbf{V}'_{\mathrm{R}}$. From eqs. (29), (30), and (33), we know that the item $\frac{\partial^2 R}{\partial \sigma^2}$ in eq. (39) can be rewritten as:

$$\frac{\partial^2 R}{\partial \sigma^2} = \frac{1}{\sin\theta}\frac{\partial v'_{\mathrm{H}}}{\partial \lambda} - \frac{1}{\sin\theta}\frac{\partial u'_{\mathrm{W}}\sin\theta}{\partial \theta}. \tag{40}$$

According to eq. (23) and the first two equations of eq. (32), we can derive:

$$\frac{1}{\sin\theta}\frac{\partial u'_{\mathrm{W}}}{\partial \lambda} + \frac{1}{\sin\theta}\frac{\partial\left(v'_{\mathrm{H}}\sin\theta\right)}{\partial \theta} = \frac{1}{\sin\theta}\frac{\partial u'}{\partial \lambda} + \frac{1}{\sin\theta}\frac{\partial(v'\sin\theta)}{\partial \theta} = D, \tag{41}$$

where D represents the divergence field of the actual atmosphere. Eq. (41) shows that the horizontal velocity u'_{W} and v'_{H} of the zonal and meridional circulation in the 3P-DGAC represent the horizontal divergent motion of the actual 3D general circulation $\mathbf{V}'$. While eq. (40) shows that $\frac{\partial^2 R}{\partial \sigma^2}$ exactly represents the component part of the actual vertical vorticity caused by the horizontal divergent motion, where the components $\frac{1}{\sin\theta}\frac{\partial v'_{\mathrm{H}}}{\partial \lambda}$ and $-\frac{1}{\sin\theta}\frac{\partial u'_{\mathrm{W}}\sin\theta}{\partial \theta}$ of $\frac{\partial^2 R}{\partial \sigma^2}$ in eq. (40) represent the vertical vorticities of the meridional and zonal circulation, respectively. These correspond to the natural relationships between different vertical layers of the actual atmosphere.

If we let $\frac{\partial^2 R}{\partial \sigma^2} = 0$, then according to eqs. (7), (8), (24), and (39) and eqs. (12), (17), (35), and (36), the horizontal circulation $\mathbf{V}_{\mathrm{R}}$ in the middle-high latitudes is equivalent to the traditional horizontal vortex circulation $\mathbf{V}_{\mathrm{rot}}$, and the meridional circulation $\mathbf{V}_{\mathrm{H}}$ and zonal circulation $\mathbf{V}_{\mathrm{W}}$ in the low latitudes are also equivalent to the Hadley and Walker circulations, respectively. Therefore, traditional 2D decomposition represents a specialized case of the 3P-DGAC.

From this theoretical analysis of the 3D Poisson eq. (39), it can be seen that, unlike the traditional 2D decomposition method, which needs to limit the motion to a certain isobaric surface, the 3P-DGAC is a 3D decomposition method for the whole atmosphere, which effectively decomposes the actual vertical vorticity into a horizontal vortex component part $\Delta_2 R$ and a divergent component part $\frac{\partial^2 R}{\partial \sigma^2}$. Thus, it provides a new potential to study the evolution of the vertical vorticity field caused by divergent motion. To verify the above theoretical analysis, Hu et al. (2017) calculated the components $\Delta_2 R$ (the first column), $\frac{\partial^2 R}{\partial \sigma^2}$ (the second column), $\Delta_2 R + \frac{\partial^2 R}{\partial \sigma^2}$ (the third column), and the climatic average (1979–2013) of ζ (the fourth column) in boreal winter (Figure 13), by using six velocity components (u_{R}, v_{R}, v_{H}, ω_{H}, u_{W}, and ω_{W}) and eqs. (38)–(40). The four rows of Figure 13 represent the results at 850, 500, and 200 hPa and the vertical average of the whole layer, respectively. Comparing the third and fourth columns of Figure 13, we find that the actual vertical vorticity ζ is approximately equal to $\Delta_2 R + \frac{\partial^2 R}{\partial \sigma^2}$, which means that the actual vertical vorticity ζ can be decomposed into the two component parts caused by the horizontal vortex circulation and the overturning divergent circulation. The second column of Figure 13 shows that the vertical vorticity caused by the divergent motion cannot be ignored in the bottom (850 hPa, Figure 13b) and top (200 hPa, Figure 13j) layer of the

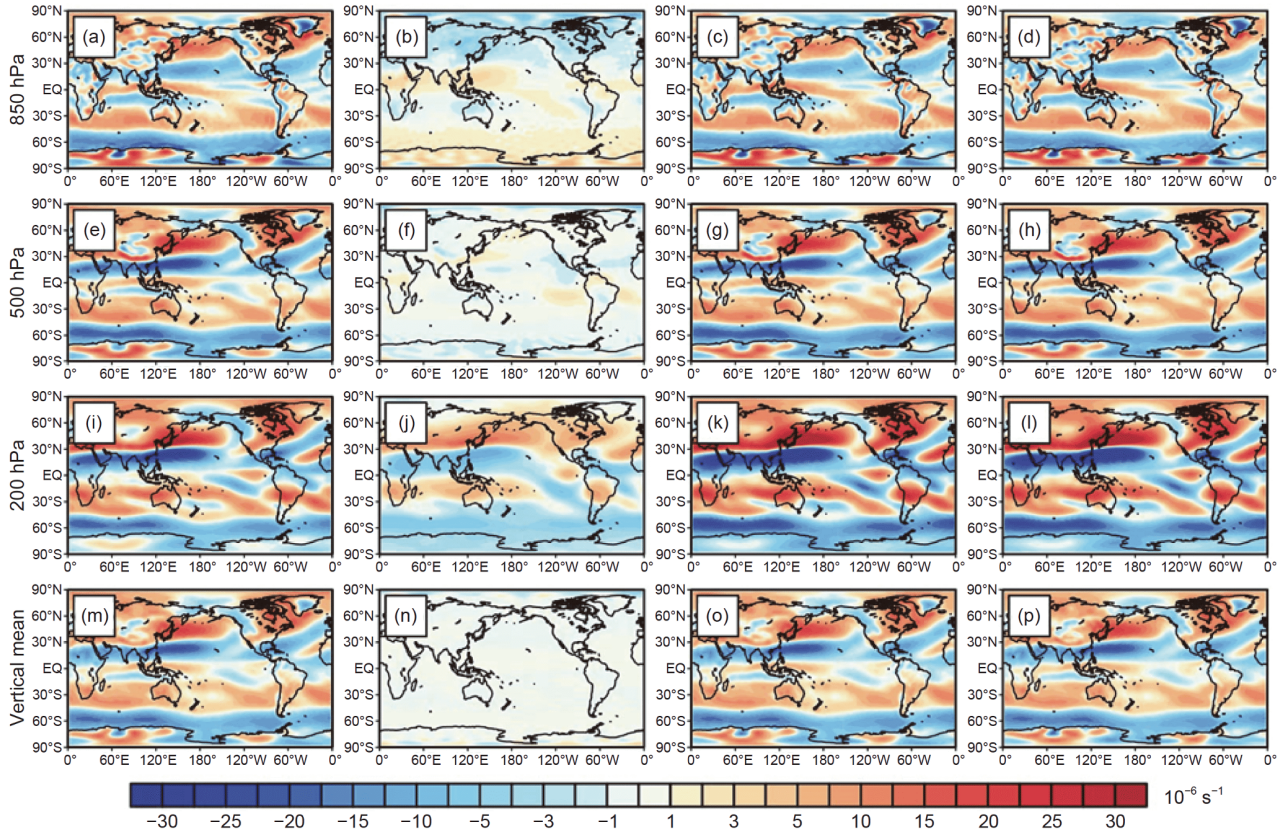

Figure 13 Climatological average characteristics of vertical vorticity ζ at 850 hPa (d) and its decomposition components $\Delta_2 R$ (a), $\frac{\partial^2 R}{\partial \sigma^2}$ (b), and $\Delta_2 R + \frac{\partial^2 R}{\partial \sigma^2}$ in boreal winter from 1979 to 2013 (c). (e)–(h), (i)–(l), and (m)–(p) are the same as (a)–(d), but for the 500 hPa, 200 hPa, and the vertical average of the whole layer. Cited from Hu et al. (2017).

troposphere, but its average value in the middle layer (500 hPa) and the entire troposphere (Figure 13n) is almost zero, which is in agreement with the classical theory that the motion at 500 hPa is quasi-horizontal and non-divergent and is often used to represent the whole layer's atmospheric motion. The characteristics of the vertical vorticity ζ and its decomposed components in other seasons are similar to those in winter, which will not be further discussed here.

4.2 Decomposition of the vertical velocity

Although vertical velocity is small, vertical movement is the key factor of all types of weather phenomena, and plays a very important role in the evolution of the general circulation. Therefore, the expression of vertical velocity has always been a significant scientific problem.

From eqs. (31) and (32) and the conversion relation (19) of the 3P-DGAC, the vertical velocity ω in the barometric coordinate system can be expressed as:

$$\begin{aligned}\omega &= P_s(\dot{\sigma}_{\mathrm{H}} + \dot{\sigma}_{\mathrm{W}}) \\ &= P_s\left(\frac{1}{\sin\theta}\frac{\partial(\sin\theta H)}{\partial\theta} - \frac{1}{\sin\theta}\frac{\partial W}{\partial\lambda}\right).\end{aligned} \tag{42}$$

The stream functions H and W are determined by the horizontal velocity field (u, v) and the stream function R by solving eqs. (35) and (36), while the stream function R is determined by solving the 3D Poisson eq. (34). Therefore, the 3P-DGAC itself provides a method for calculating the vertical velocity.

In addition, eq. (42) decomposes the vertical velocity ω into the meridional and zonal components ($\omega_{\mathrm{H}} = P_s\dot{\sigma}_{\mathrm{H}}$ and $\omega_{\mathrm{W}} = P_s\dot{\sigma}_{\mathrm{W}}$), which correspond to the vertical velocities of the 3D global meridional and zonal circulations. This is of great significance for quantitatively studying the local Hadley and Walker circulations. By analyzing the calculation results of the 3P-DGAC, Hu et al. (2017) demonstrated that, in the case of the global zonal average denoted by "[ ]", though $[\omega] = [\omega_{\mathrm{W}}] + [\omega_{\mathrm{H}}]$, the vertical velocity of the zonal circulation is zero ($[\omega_{\mathrm{W}}] = 0$), and the actual velocity $[\omega]$ only contains the component of meridional circulation (Figure 14a, 14b), which means that it is reasonable to use $[\omega]$ to represent the global zonally averaged Hadley circulation in previous research. Similarly, in the case of the global meridionally average, denoted by "< >", though $<\omega> = <\omega_{\mathrm{W}}> + <\omega_{\mathrm{H}}>$, the vertical velocity of the mer-

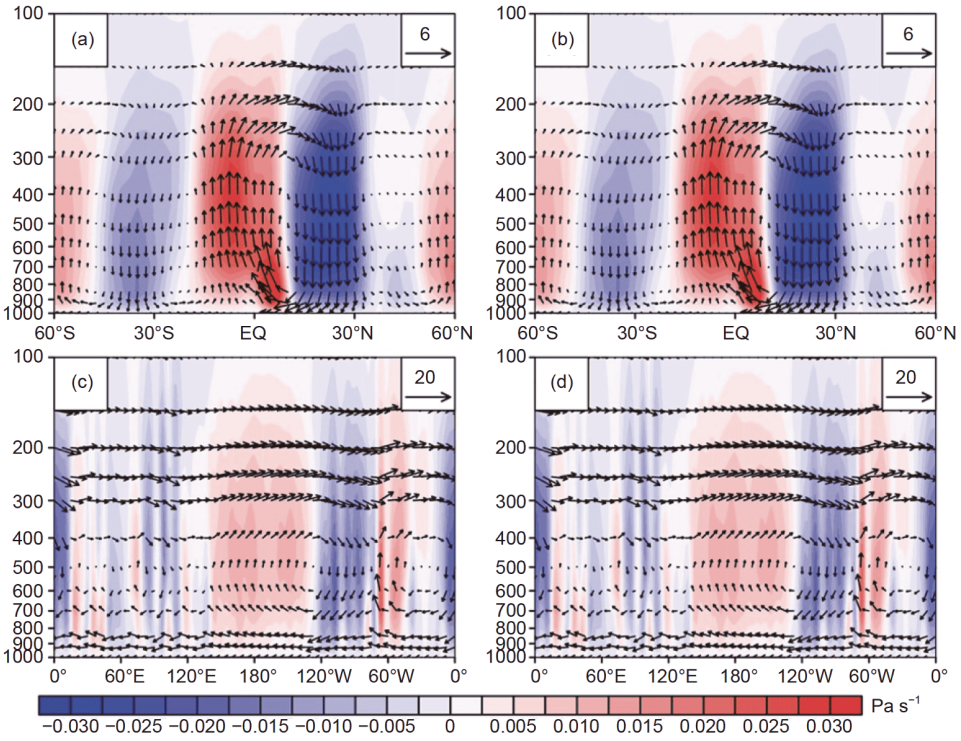

Figure 14 (a) The climatic characteristics of the global zonally averaged meridional circulation in winter (1979–2013). The vertical velocity $[\omega_H]$ is shaded, and the vectors represent the wind $(([v_H], [\omega_H]))$ with $[\omega_H]$ scaled by a factor of −100; (b) is the same as in (a), but for $[\omega]$ and $(([v_H], [\omega]))$; (c) is the same as in (a), but for the global meridionally averaged zonal circulation, where the vertical velocity $< \omega_W >$ is shaded, and the vectors represent the wind $(< u_W >, < \omega_W >)$ with $< \omega_W >$ scaled by a factor of −300; (d) is the same as in (c), but for $< \omega >$ and $(< u_W >, < \omega >)$. Cited from Hu et al. (2017).

idional circulation is zero ($< \omega_H >= 0$), and the actual vertical velocity $< \omega >$ only contains the component of zonal circulation (Figure 14c, d). However, the Walker circulation in the traditional definition is zonally vertical circulation in the tropical Pacific region; thus, we often use the meridional average of the vertical velocity ω between 5°S and 5°N (denoted by $< \omega >_{5°S}^{5°N}$) to represent the vertical velocity of the Walker circulation. However, the analysis in Figure 15 shows that $< \omega >_{5°S}^{5°N} = < \omega_H >_{5°S}^{5°N} + < \omega_W >_{5°S}^{5°N}$, but the vertical velocity of the meridional circulation is not equal to zero ($< \omega_H >_{5°S}^{5°N} \neq 0$) (Figure 15d–15f), which indicates that the contribution of the local Hadley circulation (represented by $< \omega_H >_{5°S}^{5°N}$) is included in the vertical velocity of the Walker circulation (Figure 15f). Thus, it is not accurate to use $< \omega_H >_{5°S}^{5°N}$ to represent the Walker circulation in traditional research. Similarly, the zonally average of vertical velocity ω from longitude λ_1 to λ_2 (denoted by $[\omega]_{\lambda_1}^{\lambda_2}$) is often used to represent the local Hadley circulation; thus, it is not accurate to use $[\omega]_{\lambda_1}^{\lambda_2}$ to represent the local Hadley circulation t because $[\omega]_{\lambda_1}^{\lambda_2}$ contains the vertical velocity of the Walker circulation (Figure 15a–15c). Therefore, it is more reasonable and accurate to use $[\omega_H]_{\lambda_1}^{\lambda_2}$ and $< \omega_W >_{5°S}^{5°N}$ to represent the local Hadley and local Walker circulations than to use the average value of $[\omega_H]_{\lambda_1}^{\lambda_2}$ and $< \omega_W >_{5°S}^{5°N}$ of the actual vertical velocity.

In general, the decomposition of the vertical velocity in 3P-DGAC can eliminate the effect of the meridional circulation (or zonal circulation) on the zonal circulation (or meridional circulation); thus, the decomposition formula $\omega = \omega_W + \omega_H$ is an effective way to solve the inaccuracy in representing the local Hadley circulation (or Walker circulation) caused by using $[\omega]_{\lambda_1}^{\lambda_2}$ (or using $< \omega_W >_{5°S}^{5°N}$) instead of using $[\omega_H]_{\lambda_1}^{\lambda_2}$ (or using $< \omega_W >_{5°S}^{5°N}$) in traditional studies, which is another advantage of 3P-DGAC.

5. Three-pattern decomposition of global atmospheric circulation: Dynamical equations

From the theoretical analysis of sections 2 and 3, we know that, based on the complete continuity equation, the 3P-DGAC can represent the horizontal and vertical motion components of the actual atmospheric circulations, from a global perspective. Therefore, the 3P-DGAC can be combined with the primitive equations of planetary-scale atmospheric motions, and the dynamical equations of large-scale

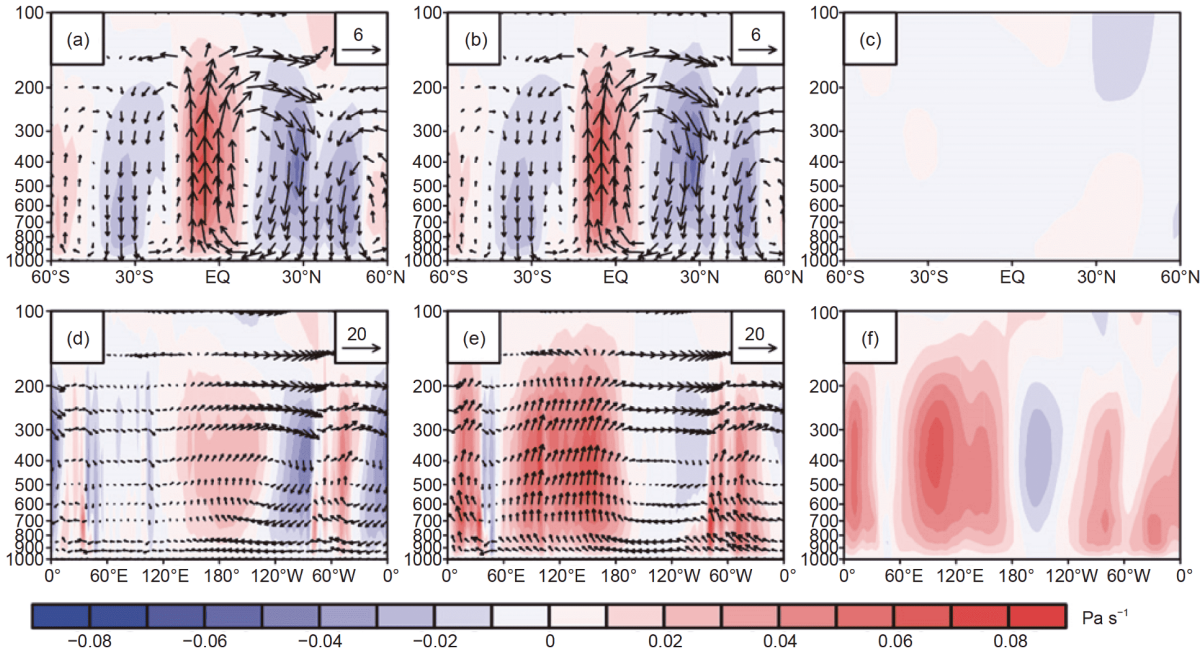

Figure 15 (a) The climatic characteristics of the local zonally averaged meridional circulation in winter (1979–2013), where the vertical velocity $[\omega_{\mathrm{H}}]_{60^{\circ}\mathrm{E}}^{140^{\circ}\mathrm{E}}$ is shaded, and the vectors represent the wind $\left([v_{\mathrm{H}}]_{60^{\circ}\mathrm{E}}^{140^{\circ}\mathrm{E}}, [\omega_{\mathrm{H}}]_{60^{\circ}\mathrm{E}}^{140^{\circ}\mathrm{E}}\right)$ with $[\omega_{\mathrm{H}}]_{60^{\circ}\mathrm{E}}^{140^{\circ}\mathrm{E}}$ scaled by a factor of −120; (b) is the same as in (a), but for $[\omega]_{60^{\circ}\mathrm{E}}^{140^{\circ}\mathrm{E}}$ and $\left([v_{\mathrm{H}}]_{60^{\circ}\mathrm{E}}^{140^{\circ}\mathrm{E}}, [\omega]_{60^{\circ}\mathrm{E}}^{140^{\circ}\mathrm{E}}\right)$. The shading of (c) represents $[\omega_{\mathrm{W}}]_{60^{\circ}\mathrm{E}}^{140^{\circ}\mathrm{E}}$; (d) is the same as in (a), but for the local meridionally averaged zonal circulation, where the shading represents $<\omega_{\mathrm{W}}>_{5^{\circ}\mathrm{S}}^{5^{\circ}\mathrm{N}}$ and the vectors represent the wind $\left(<u_{\mathrm{W}}>_{5^{\circ}\mathrm{S}}^{5^{\circ}\mathrm{N}}, <\omega_{\mathrm{W}}>_{5^{\circ}\mathrm{S}}^{5^{\circ}\mathrm{N}}\right)$ with $<\omega_{\mathrm{W}}>_{5^{\circ}\mathrm{S}}^{5^{\circ}\mathrm{N}}$ scaled by a factor of −120; (e) is the same as in (d), but for $<\omega>_{5^{\circ}\mathrm{S}}^{5^{\circ}\mathrm{N}}$ and $\left(<u_{\mathrm{W}}>_{5^{\circ}\mathrm{S}}^{5^{\circ}\mathrm{N}}, <\omega>_{5^{\circ}\mathrm{S}}^{5^{\circ}\mathrm{N}}\right)$. The shading of (f) represents $<\omega_{\mathrm{H}}>_{5^{\circ}\mathrm{S}}^{5^{\circ}\mathrm{N}}$. Cited from Hu et al. (2017).

three-pattern circulations can be established directly.

In fact, the components, eq. (32), of the 3P-DGAC can be rewritten as the following operator equation:

$$\begin{pmatrix} u' \\ v' \\ \dot{\sigma} \end{pmatrix} = \begin{pmatrix} 0 & \frac{\partial}{\partial\sigma} & -\frac{\partial}{\partial\theta} \\ -\frac{\partial}{\partial\sigma} & 0 & \frac{1}{\sin\theta}\frac{\partial}{\partial\lambda} \\ \frac{1}{\sin\theta}\frac{\partial\sin\theta}{\partial\theta} & -\frac{1}{\sin\theta}\frac{\partial}{\partial\lambda} & 0 \end{pmatrix} \begin{pmatrix} H \\ W \\ R \end{pmatrix}. \tag{43}$$

Eq. (43) shows that the velocity components (u', v' and $\dot{\sigma}$) of the actual atmosphere can be equivalently represented by the stream functions H, W and R of the horizontal, meridional, and zonal circulation, respectively, in the 3P-DGAC. Therefore, if we replace the components of the velocity field in the primitive equations of atmospheric motions using eq. (43) and keep the dissipative structure of the original system unchanged we can transform the partial differential equations of velocity field components (u', v', and $\dot{\sigma}$) in the primitive equations into the equations of the stream functions H, W, and R, which leads from the problem of predicting the velocity field in the primitive equations to the problem of directly predicting three large-scale circulations in the new dynamical equations.

The primitive equations of atmospheric motions can be rewritten as the following operator equation (Chou, 1974, 1983; Hu et al., 2018b):

$$B'\frac{\partial\phi'}{\partial t} + (N' + L')\phi' = \xi', \tag{44}$$

where $\varphi' = \frac{\varphi}{a}$ and $\phi' = (u', v', \dot{\sigma}, \varphi', T)^{\mathrm{T}}$ represent the usual atmospheric variables. $B' = \mathrm{diag}\left(a, a, 0, 0, \frac{R_0^2}{ac^2}\right)$ is a diagonal matrix, and $R_0$is the gas constant of dry air. $L' = \mathrm{diag}(\tilde{L}_1', \tilde{L}_1', 0, 0, \tilde{L}_2')$ represents the dissipative term, and $\xi' = \left(0, 0, 0, 0, \frac{R_0^2}{ac^2}\frac{\varepsilon}{c_p}\right)^{\mathrm{T}}$ represents the non-adiabatic heating process. $N'$is a nonlinear anti-adjoint operator with the following formula:

$$N' = \begin{bmatrix} a\pi' & aA' & 0 & \frac{1}{\sin\theta}\frac{\partial}{\partial\lambda} & 0 \\ -aA' & a\pi' & 0 & \frac{\partial}{\partial\theta} & 0 \\ 0 & 0 & 0 & \frac{\partial}{\partial\sigma} & \frac{R_0}{a\sigma} \\ \frac{1}{\sin\theta}\frac{\partial}{\partial\lambda} & \frac{1}{\sin\theta}\frac{\partial}{\partial\theta}\sin\theta & \frac{\partial}{\partial\sigma} & 0 & 0 \\ 0 & 0 & -\frac{R_0}{a\sigma} & 0 & \frac{R_0^2}{ac^2}\pi' \end{bmatrix},$$

where

$$\pi' = \frac{u'}{\sin\theta}\frac{\partial}{\partial\lambda} + v'\frac{\partial}{\partial\theta} + \dot{\sigma}\frac{\partial}{\partial\sigma},$$

$$A' = 2\Omega\cos\theta + \mathrm{ctg}\theta u',$$

$$\tilde{L}_1' = -a\frac{\partial}{\partial\sigma}\nu_1\left(\frac{g\sigma}{R_0\overline{T}}\right)^2\frac{\partial}{\partial\sigma} - a\mu_1\nabla^2,$$

$$\tilde{L}_2' = -\frac{1}{a}\frac{\partial}{\partial\sigma}\nu_2\left(\frac{g\sigma}{R_0\overline{T}}\right)^2\frac{\partial}{\partial\sigma} - \frac{1}{a}\mu_2\nabla^2,$$

$$c^2 = \frac{R_0^2\overline{T}}{g}(\gamma_d - \bar{\gamma}),$$

$$\nabla^2 = \frac{1}{a^2\sin^2\theta}\frac{\partial^2}{\partial\lambda^2} + \frac{1}{a^2\sin\theta}\frac{\partial}{\partial\theta}\sin\theta\frac{\partial}{\partial\theta}.$$

Here, $\overline{T} = \overline{T}(p)$ (or $\overline{\varphi'} = \overline{\varphi'}(p)$) represents the mean value (or the average of potential height) of the global average temperature on the p isobaric surface, T (or φ') represents the deviation of $\overline{T}$ or $\overline{\varphi'}$, and other variables are commonly used. The expression of the operator N' shows that it includes not only nonlinear advection and convection, but also the action of the Coriolis force and pressure gradient force. Therefore, compared with the component form of the primitive equations, the operator eq. (44) can more simply reflect the forced dissipative property of atmospheric motions (Chou, 1983).

For convenience in incorporating the 3P-DGAC into the operator eq. (44), eq. (43) must be rewritten as:

$$\phi' = C\psi$$

$$= \begin{bmatrix} 0 & \frac{\partial}{\partial\sigma} & -\frac{\partial}{\partial\theta} & 0 & 0 \\ -\frac{\partial}{\partial\sigma} & 0 & \frac{1}{\sin\theta}\frac{\partial}{\partial\lambda} & 0 & 0 \\ \frac{1}{\sin\theta}\frac{\partial}{\partial\theta}\sin\theta & -\frac{1}{\sin\theta}\frac{\partial}{\partial\lambda} & 0 & 0 & 0 \\ 0 & 0 & 0 & 1 & 0 \\ 0 & 0 & 0 & 0 & 1 \end{bmatrix}\psi, \tag{45}$$

where $\psi = (H, W, R, \varphi', T)^{\mathrm{T}}$. By substituting eq. (45) into eq. (44), we obtain:

$$CB'C\frac{\partial\psi}{\partial t} + (CN'C + CL'C)\psi = C\xi'. \tag{46}$$

Because the operator C is self-adjoint, according to the anti-adjointness of operator N' and the self-adjointness of operators B' and L' (Hu et al., 2018b), the operator $CN'C$ in eq. (46) is anti-adjoint, and operators $CB'C$ and $CL'C$ are self-adjoint. Therefore, the operator C on the left side of each term of eq. (46) maintains the operator property of eq. (44) unchanged, so that the new dynamical equations maintain the dissipative characteristics of the original planetary-scale primitive equations unchanged. Because the stream functions H, W and R are used instead of the velocity components (u', v' and $\dot{\sigma}$) in the primitive equations, we call eq. (46) the dynamical equation of large-scale three-pattern circulations (Hu et al., 2018b).

Using eq. (33), we easily obtain the components of eq. (46) as follows:

$$\frac{\partial}{\partial t}\left(-\frac{\partial^2 H}{\partial\sigma^2} + \frac{1}{\sin\theta}\frac{\partial^2 R}{\partial\lambda\partial\sigma}\right) - \frac{\partial}{\partial\sigma}\pi'\frac{\partial H}{\partial\sigma}$$
$$-\frac{\partial}{\partial\sigma}A'\frac{\partial W}{\partial\sigma} + \frac{\partial}{\partial\sigma}\left(A'\frac{\partial R}{\partial\theta} + \pi'\frac{1}{\sin\theta}\frac{\partial R}{\partial\lambda}\right)$$
$$+\frac{\partial}{a\partial\sigma}\tilde{L}_1'\left(\frac{1}{\sin\theta}\frac{\partial R}{\partial\lambda} - \frac{\partial H}{\partial\sigma}\right) = \frac{R_0}{a^2\sigma}\frac{\partial T}{\partial\theta}, \tag{47}$$

$$\frac{\partial}{\partial t}\left(\frac{\partial^2 W}{\partial\sigma^2} - \frac{\partial^2 R}{\partial\theta\partial\sigma}\right) - \frac{\partial}{\partial\sigma}A'\frac{\partial H}{\partial\sigma} + \frac{\partial}{\partial\sigma}\pi'\frac{\partial W}{\partial\sigma}$$
$$+\frac{\partial}{\partial\sigma}\left(A'\frac{1}{\sin\theta}\frac{\partial R}{\partial\lambda} - \pi'\frac{\partial R}{\partial\theta}\right) + \frac{\partial}{a\partial\sigma}\tilde{L}_1'\left(\frac{\partial W}{\partial\sigma} - \frac{\partial R}{\partial\theta}\right)$$
$$= \frac{R_0}{a^2\sigma}\frac{1}{\sin\theta}\frac{\partial T}{\partial\lambda}, \tag{48}$$

$$\frac{\partial}{\partial t}(\Delta_3 R) + \frac{1}{\sin\theta}\left(\frac{\partial}{\partial\theta}\sin\theta A'\frac{\partial H}{\partial\sigma} - \frac{\partial}{\partial\lambda}\pi'\frac{\partial H}{\partial\sigma}\right)$$
$$-\frac{1}{\sin\theta}\left(\frac{\partial}{\partial\theta}\sin\theta\pi'\frac{\partial W}{\partial\sigma} + \frac{\partial}{\partial\lambda}A'\frac{\partial W}{\partial\sigma}\right)$$
$$+\frac{1}{\sin\theta}\left(\frac{\partial}{\partial\theta}\sin\theta\pi'\frac{\partial R}{\partial\theta} + \frac{\partial}{\partial\lambda}\pi'\frac{1}{\sin\theta}\frac{\partial R}{\partial\lambda}\right.$$
$$\left.-\frac{\partial}{\partial\theta}A'\frac{\partial R}{\partial\lambda} + \frac{\partial}{\partial\lambda}A'\frac{\partial R}{\partial\theta}\right) + \frac{1}{a\sin\theta}\frac{\partial}{\partial\lambda}\tilde{L}_1'\left(\frac{1}{\sin\theta}\frac{\partial R}{\partial\lambda} - \frac{\partial H}{\partial\sigma}\right)$$
$$-\frac{1}{a\sin\theta}\frac{\partial}{\partial\theta}\sin\theta\tilde{L}_1'\left(\frac{\partial W}{\partial\sigma} - \frac{\partial R}{\partial\theta}\right) = 0, \tag{49}$$

$$\frac{R_0^2}{ac^2}\frac{\partial T}{\partial t} - \frac{R_0}{a\sigma}\left(\frac{1}{\sin\theta}\frac{\partial(\sin\theta H)}{\partial\theta} - \frac{1}{\sin\theta}\frac{\partial W}{\partial\lambda}\right)$$
$$+\frac{R_0^2}{ac^2}\pi'T + \tilde{L}_2'T = \frac{R_0^2}{ac^2}\frac{\varepsilon}{c_p}. \tag{50}$$

We note that the components of eq. (32) automatically satisfy the continuity eq. (21) of the actual atmosphere. Therefore, compared with the primitive equations, the continuity equation does not appear directly in the new eqs. (47)–(50). In fact, in the process of transformation from eq. (44) to eq. (46), by the self-adjointness of the operator C, the action process of potential height φ' in eq. (44) is transferred to the action of the temperature variable T through the state equation of air, which reduces one physical variable in eq. (46), and then reduces one equation. This makes the new dynamical eqs. (47)–(50) to be more convenient for directly studying the dynamical and thermodynamic evolution of large-scale horizontal, meridional, and zonal circulations. Furthermore, the 3D vorticity vector of the actual velocity field in the σ-coordinate system can be expressed as

$$\nabla\times\mathbf{V}' = \left(\frac{\partial\dot{\sigma}}{\partial\theta} - \frac{\partial v'}{\partial\sigma}\right)\mathbf{i} + \left(\frac{\partial u'}{\partial\sigma} - \frac{1}{\sin\theta}\frac{\partial\dot{\sigma}}{\partial\lambda}\right)\mathbf{j}$$
$$+\left(\frac{1}{\sin\theta}\frac{\partial v'}{\partial\lambda} - \frac{1}{\sin\theta}\frac{\partial(u'\sin\theta)}{\partial\theta}\right)\mathbf{k}. \tag{51}$$

By diagnosing the terms in eq. (51), we find that, com-

pared with the vertical shear $\left(-\frac{\partial v'}{\partial \sigma}\right.$ and $\left.\frac{\partial u'}{\partial \sigma}\right)$ of the horizontal velocity field, the horizontal shear terms $\left(\frac{\partial \dot{\sigma}}{\partial \theta}\right.$ and $\left.-\frac{1}{\sin\theta}\frac{\partial \dot{\sigma}}{\partial \lambda}\right)$ of the vertical velocity of large-scale motions are small. Therefore, if we use $-\frac{\partial v'}{\partial \sigma}$ and $\frac{\partial u'}{\partial \sigma}$ to approximate the zonal and the meridional vorticities, respectively, eq. (51) can be approximated as follows:

$$\begin{aligned}\nabla\times\mathbf{V}' &= \zeta_\lambda\mathbf{i}+\zeta_\theta\mathbf{j}+\zeta_\sigma\mathbf{k}\\ &\cong -\frac{\partial v'}{\partial\sigma}\mathbf{i}+\frac{\partial u'}{\partial\sigma}\mathbf{j}+\left(\frac{1}{\sin\theta}\frac{\partial v'}{\partial\lambda}-\frac{1}{\sin\theta}\frac{\partial(u'\sin\theta)}{\partial\theta}\right)\mathbf{k},\end{aligned} \tag{52}$$

where ζ_λ, ζ_θ, and ζ_σ represent the zonal, meridional, and vertical vorticities, respectively. By using eqs. (24), (29), (30), and (52), we can easily rewrite the dynamical eqs. (47)–(49) of the three-pattern circulation into the following 3D vorticity equations:

$$\begin{aligned}\frac{\partial\zeta_\lambda}{\partial t} &= -\pi'\zeta_\lambda-\zeta_\lambda D_\lambda+\frac{1}{\sin\theta}\frac{\partial v'}{\partial\lambda}\frac{\partial u'}{\partial\sigma}-f\xi_\theta\\ &\quad-\left(2\mathrm{ctg}\theta u'\frac{\partial u'}{\partial\sigma}+\mathrm{ctg}\theta v'\frac{\partial v'}{\partial\sigma}\right)+\frac{\partial}{a\partial\sigma}\tilde{L}_1'v'-\frac{R_0}{a^2\sigma}\frac{\partial T}{\partial\theta},\end{aligned} \tag{53}$$

$$\begin{aligned}\frac{\partial\zeta_\theta}{\partial t} &= -\pi'\zeta_\theta-\zeta_\theta D_\theta-\frac{1}{\sin\theta}\frac{\partial u'\sin\theta}{\partial\theta}\frac{\partial v'}{\partial\sigma}+f\zeta_\lambda\\ &\quad-\mathrm{ctg}\theta v'\frac{\partial u'}{\partial\sigma}-\frac{\partial}{a\partial\sigma}\tilde{L}_1'u'+\frac{R_0}{a^2\sigma}\frac{1}{\sin\theta}\frac{\partial T}{\partial\lambda},\end{aligned} \tag{54}$$

$$\begin{aligned}\frac{\partial\zeta_\sigma}{\partial t} &= -\pi'\zeta_\sigma-\pi'(-f)-\zeta_\sigma D_\sigma\\ &\quad-(-f)D_\sigma+\left(\frac{\partial\dot{\sigma}}{\partial\theta}\zeta_\theta+\frac{1}{\sin\theta}\frac{\partial\dot{\sigma}}{\partial\lambda}\zeta_\lambda\right)\\ &\quad+\left(\frac{1}{a\sin\theta}\frac{\partial}{\partial\theta}\sin\theta\tilde{L}_1'u'-\frac{1}{a\sin\theta}\frac{\partial}{\partial\lambda}\tilde{L}_1'v'\right),\end{aligned} \tag{55}$$

where $D_\lambda=\frac{1}{\sin\theta}\frac{\partial v'\sin\theta}{\partial\theta}+\frac{\partial\dot{\sigma}}{\partial\sigma}$ and $D_\theta=\frac{1}{\sin\theta}\frac{\partial u'}{\partial\lambda}+\frac{\partial\dot{\sigma}}{\partial\sigma}$ represent the divergence in the meridional and zonal planes, respectively, and $D_\sigma=\frac{1}{\sin\theta}\frac{\partial u'}{\partial\lambda}+\frac{1}{\sin\theta}\frac{\partial v'\sin\theta}{\partial\theta}$ represents the horizontal divergence. A detailed explanation of the physical meanings of eqs. (53)–(55) can be found in (Hu et al., 2018b).

The dynamical equations of large-scale horizontal, meridional, and zonal circulation, which are obtained by combining the 3P-DGAC with the primitive equations of atmospheric motion, not only reveal the dynamic mechanisms of evolution of large-scale 3D circulations from the perspective of the evolution of the 3D vorticity field (i.e., zonal, meridional, and vertical vorticities), but also provide the source terms of the nonlinear interactions among the large-scale three-pattern circulations from the perspective of the decomposition of the vorticity field (Hu et al., 2018b). From eqs. (32) and (52), the 3D vorticity components of the velocity field $\mathbf{V}'$ can be rewritten as:

$$\begin{cases}\zeta_\lambda=\zeta_{\lambda H}+\zeta_{\lambda R}\cong\left(-\frac{\partial v'_{\mathrm{H}}}{\partial\sigma}\right)+\left(-\frac{\partial v'_{\mathrm{R}}}{\partial\sigma}\right),\\ \zeta_\theta=\zeta_{\theta W}+\zeta_{\theta R}\cong\frac{\partial u'_{\mathrm{W}}}{\partial\sigma}+\frac{\partial u'_{\mathrm{R}}}{\partial\sigma},\\ \zeta_\sigma=\zeta_{\sigma R}+\zeta_{\sigma H}+\zeta_{\sigma W}\\ =\left(\frac{1}{\sin\theta}\frac{\partial v'_{\mathrm{R}}}{\partial\lambda}-\frac{1}{\sin\theta}\frac{\partial(u'_{\mathrm{R}}\sin\theta)}{\partial\theta}\right)\\ +\frac{1}{\sin\theta}\frac{\partial v'_{\mathrm{H}}}{\partial\lambda}-\frac{1}{\sin\theta}\frac{\partial(u'_{\mathrm{W}}\sin\theta)}{\partial\theta},\end{cases} \tag{56}$$

where $\zeta_{\lambda H}$ and $\zeta_{\lambda R}$ represent the zonal vorticity components of the meridional and horizontal circulations, $\zeta_{\theta W}$ and $\zeta_{\theta R}$ represent the meridional vorticity components of the zonal and horizontal circulations, respectively, while $\zeta_{\sigma R}$, $\zeta_{\sigma H}$and $\zeta_{\sigma W}$ represent the vertical vorticity components of the horizontal, meridional, and zonal circulations, respectively. If we substitute the expressions of the decomposition components of 3D vorticity (ζ_λ, ζ_θ, and ζ_σ) in eq. (56) into eqs. (53)–(55), the decomposition formulas of eqs. (53)–(55) were obtained. By diagnosing and analyzing the decomposition formulas of the 3D vorticity equations, we can quantitatively reveal the dynamical mechanism of the nonlinear source term effect of the large-scale three-pattern circulations under the background of global warming, especially the direct action mechanism of the temperature gradients $\frac{R_0}{a^2\sigma}\frac{\partial T}{\partial\theta}$ and $\frac{R_0}{a^2\sigma}\frac{1}{\sin\theta}\frac{\partial T}{\partial\lambda}$ caused by uneven global warming on the generation and development of meridional and zonal circulations.

6. Conclusions

According to the main characteristics of atmospheric motion, we often divide the actual atmospheric circulation into middle-high latitude circulation and low latitude atmospheric circulation, which leads to an erroneous consideration of the separation of these two subjects: middle-high and low latitude atmospheric dynamics. In fact, atmospheric motions around the rotating earth must be treated as a whole. There are complex interactions between low latitude and middle-high latitude atmospheric circulations, so it is an important scientific problem to study the 3D motion law governing atmospheric circulations from a global perspective.

The theoretical framework of 3P-DGAC introduced in this paper is a new theory for solving the dynamics of the unified description of global atmospheric circulation. Through theoretical analysis and calculation results of reanalysis data, we found that the 3P-DGAC not only decomposes the actual large-scale circulation into the superposition of horizontal, meridional, and zonal circulations, but also separates the

meridional and zonal circulation parts from the vertical velocity of the actual atmosphere and the horizontal and convergence/divergence parts from the vertical vorticity (Hu et al., 2017). Among these, the effective separation of the meridional and zonal circulation components from the actual vertical velocity provides a feasible method to overcome the inaccuracy of the calculation results caused due to the actual vertical velocity being used to represent the local zonal vertical circulation (or the meridional vertical circulation) in traditional research. Nevertheless, the vertical velocity of local zonal vertical circulation contains meridional vertical circulation (or zonal vertical circulation). The decomposition of vertical vorticity not only provides a novel method to study the evolution of the vertical vorticity field caused by convergence and divergence, but it also decomposes the dynamical equations of global horizontal, meridional, and zonal circulations (Hu et al., 2018b). It can therefore be used to diagnose and analyze complex source-term processes of nonlinear interactions among the three-pattern large-scale circulations by using 3P-DGAC and the new dynamical equations to reveal the dynamical mechanisms under the background of global warming. In particular, it provides a new theoretical tool for studying the direct action mechanism of the temperature gradient caused by uneven global warming on the generation and development of meridional and latitudinal circulations.

The 3P-DGAC is a 3D decomposition method based on the characteristics of actual atmospheric motions. Since horizontal, meridional, and zonal circulations derived from the 3P-DGAC are global generalizations of Rossby waves in the middle-high latitude and Hadley and Walker circulations in the low latitudes, respectively, the new circulation decomposition model and its dynamical equations have potential application value in the quantitative diagnosis and research on the mechanisms of the complex interactions between the middle-high and low latitude atmospheric circulations. Furthermore, they also allow exploration of novel ideas and methods for research on the physical mechanism of the abnormal evolution of Rossby waves, Hadley circulation, and Walker circulation.

Acknowledgements *The authors wish to thank reviewers for their valuable comments and constructive suggestions, which significantly improved the paper. This work was supported by the National Key R & D Program of China (Grant No. 2017YFC1502305) and the National Natural Science Foundation of China (Grant Nos. 41775069 & 41975076).*

References

Bayr T, Dommenget D, Martin T, Power S B. 2014. The eastward shift of the Walker Circulation in response to global warming and its relationship to ENSO variability. Clim Dyn, 43: 2747–2763

Charney J, Halem M, Jastrow R. 1969. Use of incomplete historical data to infer the present state of the atmosphere. J Atmos Sci, 26: 1160–1163

Chelton D B, Schlax M G. 1996. Global observations of oceanic Rossby waves. Science, 272: 234–238

Cheng J B. 2019. Changes of the Hadley circulation and the influence of orography on them derived from the three-pattern decomposition of global atmospheric circulation (in Chinese). Dissertation for Doctoral Degree. Lanzhou: Lanzhou University

Cheng J B, Gao C B, Hu S J, Feng G L. 2018a. High-stability algorithm for the three-pattern decomposition of global atmospheric circulation. Theor Appl Climatol, 133: 851–866

Cheng J B, Hu S J, Chou J F. 2018b. The double-layer structure of the Hadley circulation and its interdecadal evolution characteristcs. J Trop Meteorol, 24: 220–231

Chou J F. 1974. A problem of using past data in numerical weather forecasting (in Chinese). Sci China Ser A, 6: 635–644

Chou J F. 1983. Some properties of operators and the effect of initial condition (in Chinese). Acta Meteorol Sin, 41: 385–392

Deng B S, Liu H T, Chou J F. 2010. An analysis on large-scale air-sea interactive linkages between the tropical Indian Ocean and the Pacific Ocean during ENSO events. J Trop Meteorol, 16: 305–312

DiNezio P N, Vecchi G A, Clement A C. 2013. Detectability of changes in the Walker circulation in response to global warming. J Clim, 26: 4038–4048

England M H, McGregor S, Spence P, Meehl G A, Timmermann A, Cai W, Gupta A S, McPhaden M J, Purich A, Santoso A. 2014. Recent intensification of wind-driven circulation in the Pacific and the ongoing warming hiatus. Nat Clim Change, 4: 222–227

Guan X, Ma J, Huang J, Huang R, Zhang L, Ma Z. 2019. Impact of oceans on climate change in drylands. Sci China Earth Sci, 62: 891–908

Hartmann D L. 1994. Global Physical Climatology. San Diego: Academic Press. 155

Holton J R, Staley D O. 1973. An introduction to dynamic meteorology. Am J Phys, 41: 752–754

Hou X Y, Cheng J B, Hu S J, Feng G L. 2018. Interdecadal variations in the Walker circulation and its connection to inhomogeneous air temperature changes from 1961–2012. Atmosphere, 9: 469

Hu S J. 2006. Three-dimensional circulation expansion of global atmospheric circumfluence and characteristics analyze of atmospheric vertical motion (in Chinese). Dissertation for Doctoral Degree. Lanzhou: Lanzhou University

Hu S J. 2008. Connection between the short period evolution structure and vertical motion of the subtropical high pressure in July 1998 (in Chinese). J Lanzhou Univ, 44: 28–32

Hu S J, Cheng J B, Chou J F. 2017. Novel three-pattern decomposition of global atmospheric circulation: Generalization of traditional two-dimensional decomposition. Clim Dyn, 49: 3573–3586

Hu S J, Chou J F, Cheng J B. 2018a. Three-pattern decomposition of global atmospheric circulation: Part I—Decomposition model and theorems. Clim Dyn, 50: 2355–2368

Hu S J, Cheng J B, Xu M, Chou J F. 2018b. Three-pattern decomposition of global atmospheric circulation: Part II—Dynamical equations of horizontal, meridional and zonal circulations. Clim Dyn, 50: 2673–2686

Hu Y Y, Tung K K, Liu J P. 2005. A closer comparison of early and late-winter atmospheric trends in the northern hemisphere. J Clim, 18: 3204–3216

Hu Y Y, Fu Q. 2007. Observed poleward expansion of the Hadley circulation since 1979. Atmos Chem Phys, 7: 5229–5236

Hu Y Y, Huang H, Zhou C. 2018. Widening and weakening of the Hadley circulation under global warming. Sci Bull, 63: 640–644

Kiladis G N, Weickmann K M. 1992a. Circulation anomalies associated with tropical convection during northern winter. Mon Weather Rev, 120: 1900–1923

Kiladis G N, Weickmann K M. 1992b. Extratropical forcing of tropical Pacific convection during northern winter. Mon Weather Rev, 120: 1924–1939

Kiladis G N, Feldstein S B. 1994. Rossby wave propagation into the tropics in two GFDL general circulation models. Clim Dyn, 9: 245–252

Kiladis G N, Wheeler M. 1995. Horizontal and vertical structure of observed tropospheric equatorial Rossby waves. J Geophys Res, 100: 22981–22997

Kiladis G N, Weickmann K M. 1997. Horizontal structure and seasonality of large-scale circulations associated with submonthly tropical convection. Mon Weather Rev, 125: 1997–2013
Kosaka Y, Xie S P. 2013. Recent global-warming hiatus tied to equatorial Pacific surface cooling. Nature, 501: 403–407
Liu H T, Hu S J, Xu M, Chou J F. 2008. Three-dimensional decomposition method of global atmospheric circulation. Sci China Ser D-Earth Sci, 51: 386–402
Mitas C M, Clement A. 2005. Has the Hadley cell been strengthening in recent decades? Geophys Res Lett, 32: L03809
Oort A H, Yienger J J. 1996. Observed interannual variability in the Hadley circulation and its connection to ENSO. J Clim, 9: 2751–2767
Qian W H, Wu K J, Chen D L. 2015. The Arctic and Polar cells act on the Arctic sea ice variation. Tellus Ser A-Dyn Meteorol Oceanol, 67: 27692
Qian W H, Wu K J, Liang H Y. 2016. Arctic and Antarctic cells in the troposphere. Theor Appl Climatol, 125: 1–12
Qian W H, Wu K J, Leung J C H. 2017. Climatic anomalous patterns associated with the Arctic and Polar cell strength variations. Clim Dyn, 48: 169–189
Rossby C G. 1939. Relation between variations in the intensity of the zonal circulation of the atmosphere and the displacements of the semi-permanent centers of action. J Mar Res, 2: 38–55
Schwendike J, Govekar P, Reeder M J, Wardle R, Berry G J, Jakob C. 2014. Local partitioning of the overturning circulation in the tropics and the connection to the Hadley and Walker circulations. J Geophys Res-Atmos, 119: 1322–1339
Schwendike J, Berry G J, Reeder M J, Jakob C, Govekar P, Wardle R. 2015. Trends in the local Hadley and local Walker circulations. J Geophys Res-Atmos, 120: 7599–7618
Tao Z Y, Zhou X G, Zheng Y G. 2012. Theoretical basis of weather forecasting: Quasi-geostrophic theory summary and operational applications (in Chinese). Adv Meteorol Sci Technol, 2: 6–16
Trenberth K E, Stepaniak D P. 2003. Seamless poleward atmospheric energy transports and implications for the Hadley circulation. J Clim, 16: 3706–3722
Trenberth K E, Caron J M. 2001. Estimates of meridional atmosphere and ocean heat transports. J Clim, 14: 3433–3443
Wu G X, Stefano T. 1988. A scheme for calculating the mean meridional circulation of the atmosphere (in Chinese). Sci China Ser B, 18: 106–114
Xu M. 2001. Study on the three dimensional decomposition of large scale circulation and its dynamical feature (in Chinese). Dissertation for Doctoral Degree. Lanzhou: Lanzhou University
Zhang C, Webster P J. 1992. Laterally forced equatorial perturbations in a linear model. Part I: Stationary transient forcing. J Atmos Sci, 49: 585–607
Zhou X G, Wang X M, Tao Z Y.2013. Review and discussion of some basic problems of the quasi-geostrophic theory (in Chinese). Meteorol Mon, 39: 401–409

(Responsible editor: Dehai LUO)